Microbial byproducts determine reproductive fitness of free-living and parasitic nematodes

Mericien Venzon[*1,2], Ritika Das[*2,4], Daniel J. Luciano[2,5], Julia Burnett[2], Hyun Shin Park[6], Joseph Cooper Devlin[5], Eric T. Kool[7], Joel G. Belasco[2,5], E. Jane Albert Hubbard[2,3,4,†], Ken Cadwell[2,5,8,†]

1. Vilcek Institute of Graduate Biomedical Sciences, New York University Grossman School of Medicine, New York, NY, USA
2. Kimmel Center for Biology and Medicine at the Skirball Institute, New York University Grossman School of Medicine, New York, NY, USA
3. Department of Pathology, New York University Grossman School of Medicine, New York, NY, USA
4. Department of Cell Biology, New York University Grossman School of Medicine, New York, NY, USA
5. Department of Microbiology, New York University Grossman School of Medicine, New York, NY, USA
6. Seegene Inc., Ogeum-ro, Songpa-Gu, Seoul, Republic of Korea
7. Department of Chemistry, Stanford Cancer Institute and ChEM-H Institute, Stanford University, Stanford, CA, USA
8. Division of Gastroenterology, Department of Medicine, New York University Grossman School of Medicine, New York, NY, USA

* These authors contributed equally

[†]Co-corresponding, equal contribution

Correspondence:

jane.hubbard@nyulangone.org

ken.cadwell@nyulangone.org

Summary

A distinguishing feature of *Trichuris* nematodes is that these parasitic worms reproduce within the digestive tracts of humans and other mammalian hosts shedding thousands of eggs daily, facilitating their sustained presence in the environment and hampering eradication efforts. Although this aspect of the lifecycle places *Trichuris* in a microbiota-rich environment, metabolic byproducts of bacteria that facilitate the reproductive development of parasites are unknown. Here, we employ a pipeline using the well-characterized free-living nematode *C. elegans* to identify microbial factors with conserved roles in the reproduction of nematodes. A screen for *E. coli* mutants that impair *C. elegans* fertility identified genes in fatty acid biosynthesis and ethanolamine utilization pathways, including *fabH* and *eutN*. *Trichuris muris* eggs displayed defective hatching in the presence of *E. coli* deficient in *fabH* or *eutN* due to reduction in arginine or elevated levels of aldehydes, respectively. Remarkably, *T. muris* reared in gnotobiotic mice colonized with these *E. coli* mutants displayed profound abnormalities including morphological defects and a failure to lay viable eggs. These findings indicate that microbial byproducts mediate evolutionarily conserved transkingdom interactions that impact the reproductive fitness of distantly-related nematodes.

Introduction

The reproductive success of the parasitic nematode *Trichuris trichiura* is evidenced by the over 400 million individuals colonized by this soil-transmitted helminth (Vos et al., 2016). Its enormous reproductive capacity contributes to its infectious spread and hampers parasite eradication efforts. A distinct feature of *Trichuris* species is that reproductive development, from egg hatching to egg laying, is completed exclusively within the host digestive tract (Fahmy, 1954; Panesar, 1989). A new infection begins when embryonated eggs ingested from the environment hatch in the host cecum, a region within the gastrointestinal tract populated by a dense community of bacteria. Although bacteria mediate egg hatching for *Trichuris muris* (Hayes et al., 2010; Koyama, 2016; White et al., 2018), the *Trichuris* species that infects mice, a role for bacteria at later stages of *Trichuris* development remains unclear. Our group and others have shown that *Trichuris* infections in mice and humans affect the bacterial composition of the gut microbiota (Holm et al., 2015; Houlden et al., 2015; Jenkins et al., 2017; Lee et al., 2014; Ramanan et al., 2016; Rosa et al., 2021; Schachter et al., 2020; White et al., 2018). Additionally, the *T. muris* microbiota harbors taxa similar to those observed in the murine host microbiota, with a notable enrichment of Proteobacteria, including Gram-negative commensals like *E. coli* (White et al., 2018).

For the free-living nematode *C. elegans*, reducing the quantity or quality of the bacterial diet, or interfering with nutrient uptake, can impair germline development with consequences for fertility (Dalfo et al., 2012; Gracida and Eckmann, 2013; Korta et al., 2012; Pekar et al., 2017; Spanier et al., 2018; Starich et al., 2020). Because of the high degree of conservation of body plan and neuromuscular system organization within the

69 phylum Nematoda, *C. elegans* has been used as a model for the discovery of
70 anthelmintics for more than four decades (Salinas and Risi, 2018; Sepulveda-Crespo et
71 al., 2020). Therefore, we hypothesized that bacteria-derived essential requirements for
72 reproductive development in the well-characterized, model organism *C. elegans* are
73 conserved in *Trichuris*.

74 **Results**

75 **High-throughput screen identifies *E. coli* mutants that delay *C. elegans* fertility**

76 To identify bacteria-derived factors that impact nematode reproduction, we
77 assessed fertility of young adult *C. elegans* raised in 96-well format on a library of viable
78 *E. coli* mutants suspended in liquid media. We used *C. elegans* bearing a temperature-
79 sensitive mutation in the gene encoding the GLP-1 Notch receptor, *glp-1(e2141),* to
80 facilitate quantification of fertility. At the semi-permissive temperature of 20ºC, the
81 number of germline progenitor cells is roughly half of the wild type (Michaelson et al.,
82 2010), thereby sensitizing the worms to fertility defects when signaling pathways
83 conveying nutritional sufficiency are altered (Dalfo et al., 2012; Korta et al., 2012). The
84 *C. elegans* strain also carried fluorescent markers for the pharynx and for embryos (Roy
85 et al., 2018) to facilitate counting and staging the worms, and to determine whether
86 individual worms contained embryos (gravid) (Fig. 1, A-B). Wells were excluded from
87 subsequent analyses if *E. coli* failed to grow, or if *C. elegans* exhibited developmental
88 arrest or severely delayed growth. Using a series of selection criteria that considered
89 both plate-by-plate statistical comparisons and penetrance, our primary screen of ~3000
90 of the 3985 *E. coli* mutants in the Keio library identified 315 bacterial mutants that
91 reduced the percentage of gravid worms at the established time point (Fig. 1C).

92 After these 315 *E. coli* mutants were re-screened in biological triplicate, ten
93 mutants significantly reduced the penetrance of embryo-bearing *C. elegans* compared
94 to our wild-type (WT) *E. coli* control strain (GC1547) in at least two out of three
95 biological replicates (Fig. 1C and S1, A-C). Seven of the ten *E. coli* genes fell into three
96 functional groups related to ethanolamine utilization, fatty acid biosynthesis or
97 lipopolysaccharide synthesis (Table S1). We focused on the *E. coli* mutants associated
98 with the two functional groups fatty acid biosynthesis and ethanolamine utilization:
99 *ΔfabF, ΔfabH, ΔeutD,* and *ΔeutN*. We pursued these functional groups because there
100 were two mutants each that affected these processes and these mutants displayed
101 consistent results across experiments, increasing our confidence that they represented
102 bona fide hits (Fig. 1D). Complementation of the Δ*fabH*, Δ*eutN,* and Δ*eutD* mutations
103 with a plasmid-borne copy of the corresponding gene confirmed their functional
104 relevance in the *C. elegans* fertility delay phenotype (Fig. S1D-E). For Δ*fabF*, we
105 rederived the *E. coli* deletion mutant by using P1 phage to transduce the original
106 Δ*fabF*::*kan* allele from the Keio library strain into the Keio progenitor strain BW25113
107 (Fig. S1, F-G). Similar to the original mutant, the transductant caused a significant
108 reduction in the percentage of embryo-bearing *C. elegans*.
109 To assess whether these *E. coli* mutants caused delays in somatic and/or
110 germline development of *C. elegans*, we performed two different assays. First, we
111 assayed somatic development using a time-course analysis of vulval development (Mok
112 et al., 2015). Among the four mutants, only worms fed *ΔeutN* exhibited delayed somatic
113 development (Fig. 1E). We also assayed for a delay in germline relative to somatic
114 development (Fig. 1F) using as an assay enhancement of the temperature-sensitive Pro

115 phenotype seen in a weak *glp-1(gf)* mutant (Pepper et al., 2003). Enhancement of Pro
116 at the permissive temperature often occurs as a result of delayed germline development
117 relative to somatic development (Hubbard and Schedl, 2019). Taken together, within the
118 limits of these two assays we infer that the soma and germline of worms fed *⊿fabH*
119 developed comparably with worms fed WT *E. coli, ⊿fabF* and *⊿eutD* displayed delayed
120 germline development without a somatic delay, and Δ*eutN* delayed somatic
121 development as well as germline development relative to the (already delayed) somatic
122 development.

123 Because our screen assessed the proportion of gravid *C. elegans* at a single
124 time point, we asked whether non-gravid worms were permanently sterile or were
125 delayed in achieving fertility. Exact time points corresponding to larval development
126 differ when *C. elegans* is grown in liquid versus on solid media. Our screening time
127 point ("Day 1" 62-65 hours post seeding; see Methods) is an early adult timepoint when
128 worms fed on the WT bacteria are virtually all gravid (excluding a low background
129 sterility of GC1474). When we prolonged the assay by scoring the worms on Day 2—24
130 hours after the initial screening time point—the percentage of gravid worms significantly
131 increased, indicating that feeding on these *E. coli* mutants delayed *C. elegans* fertility
132 rather than induced permanent sterility (Fig. 1G). We also found no significant
133 differences when comparing the number of germline progenitor zone (PZ) nuclei in *C.*
134 *elegans* raised on each mutant or WT *E. coli* at the L4-to-adult molt (Fig. S1, H-I),
135 indicating that the delay in fertility is not likely due to slower accumulation of the PZ
136 during larval stages (Agarwal et al., 2018; Kocsisova et al., 2019; Korta et al., 2012).

137 DAF-2 insulin/IGF-like and DAF-7 TGFß signaling pathways promote germline
138 progenitor expansion and fertility in response to adequate nutrition, and this effect is
139 also observed in the *glp-1* mutant background used in our screen (Dalfo et al., 2012;
140 Michaelson et al., 2010; Pekar et al., 2017; Starich et al., 2020). Activation of these
141 pathways ultimately interferes with the activity of downstream transcriptional regulators,
142 *daf-16* and *daf-5*, respectively; loss of *daf-16* or *daf-5* therefore mimics constitutive
143 activation of these pathways. We wished to determine whether loss of *daf-16* or *daf-5,*
144 neither of which alter overall growth rate, would circumvent the fertility delay caused by
145 each of the *E. coli* mutant diets. We fed WT or mutant *E. coli* to *daf-16* and *daf-5* mutant
146 *C. elegans* and determined the percentage of gravid worms. Loss of *daf-16* actually
147 exacerbated instead of rescuing the fertility defect of *C. elegans* raised on each mutant
148 *E. coli*, as well as on WT *E. coli* (Fig. S1J). Although constitutive activation of the DAF-7
149 TGFß pathway via loss of *daf-5* partially and variably suppressed the fertility defect of *C.*
150 *elegans* raised on *ΔeutN*, *ΔfabF* and *ΔfabH* (Fig. S1K), it also elevated the penetrance
151 of gravid *C. elegans* raised on WT *E. coli* to a similar extent, making the suppression
152 difficult to interpret. In short, we do not observe a simple causal relationship between
153 either the insulin or TGFß signaling pathways as assayed by loss of *daf-16* or *daf-5*, and
154 the alteration in the timing of *C. elegans* fertility caused by these four *E. coli* mutants.
155

156 **_E. coli_ mutants with altered metabolic byproducts delay _C. elegans_ fertility and**
157 **inhibit _T. muris_ egg hatching**

158 Having identified *E. coli* mutants that delay fertility of a free-living nematode, we
159 examined whether these bacteria impact a distantly related parasitic nematode. *T. muris*

160 egg hatching was shown to be the reproductive stage sensitive to the presence of
161 bacteria (Hayes et al., 2010; White et al., 2018). Thus, to begin investigating possible
162 effects of the mutants identified in our *C. elegans* screen on the *Trichuris* lifecycle, we
163 adapted a previously described method to quantify *E. coli*-mediated hatching kinetics of
164 embryonated *T. muris* eggs *in vitro* (Hayes et al., 2010) (Fig. 2A). All *E. coli* mutants
165 were confirmed to have similar growth kinetics to WT *E. coli* (Fig. S2A). Two of the
166 mutants tested, *ΔeutN* and *ΔfabH,* elicited significantly reduced hatching compared to
167 rates mediated by WT *E. coli* (Fig. 2B). Complementation of *ΔeutN* or *ΔfabH* with a
168 plasmid-borne copy of the corresponding gene rescued hatching (Fig. S2, B-C).
169 To determine whether reduced egg hatching is due to the production of a toxic
170 factor, we performed the hatching assay utilizing WT *E. coli* mixed with each mutant
171 (Fig. 2C). As little as 10% *ΔeutN* in the mixture significantly inhibited the ability of WT *E.*
172 *coli* to mediate hatching, whereas the presence of *ΔfabH* had no effect. Thus, the
173 inhibitory effect of *ΔeutN* is dominant over WT *E. coli*, implicating the production of a
174 toxic factor by this mutant, while the reduced hatching rate of embryonated eggs
175 incubated with *ΔfabH* is likely due to deficiency of a pro-hatching factor.
176 Hybrid metabolomics revealed an unexpectedly low relative level of arginine and
177 ornithine in *ΔfabH* cell lysates compared to WT *E. coli* (Fig. 2D). Although interactions
178 between the fatty acid and arginine biosynthesis pathways of *E. coli* have not been
179 previously described, *fabH* deficiency would cause a buildup of its substrate malonyl-
180 ACP. A possible consequence of this buildup is compensatory decreased cycling of
181 acetyl-CoA, particularly through the TCA cycle, and consequential slowing of the urea
182 cycle and arginine biosynthesis. Supplementation of *ΔfabH* cultures with arginine or

183 ornithine successfully rescued *T. muris* egg hatching to levels similar to WT *E. coli* (Fig.
184 2, E-F). Similarly, supplementation of *ΔfabH* cultures with arginine or ornithine
185 significantly increased *C. elegans* fertility (Fig. S2, D-E). Consistent with a role for the
186 arginine biosynthesis pathway, we found that *Trichuris* egg hatching was diminished in
187 the presence of *ΔargE* or *ΔargH E. coli*, mutants defective in ornithine and arginine
188 synthesis, respectively (Fig. 2, G-H).

189 Although optimal *T. muris* egg hatching *in vitro* requires physical contact with *E.*
190 *coli* (Hayes et al., 2010; Koyama, 2016), a reduced amount of hatching can still occur in
191 a transwell system that separates bacteria and eggs into different chambers (Koyama,
192 2016), suggesting that both contact-dependent and independent factors contribute to
193 the process. Similar to previous reports, eggs hatched at approximately 50% their
194 maximum rate when incubated separately from WT *E. coli* in a transwell system (Fig. 2,
195 I-J). Hatching was further reduced when *ΔfabH* was used as the bacterium.
196 Supplementation of ornithine restored hatching in the presence of *ΔfabH* to levels
197 similar to those elicited by WT *E. coli* in the transwell system. Altogether, these findings
198 indicate that nematode pathways regulated by ornithine and arginine contribute to
199 contact-independent *E. coli*-mediated hatching of *T. muris* embryonated eggs.
200

201 **Toxic intermediates of the *E. coli* ethanolamine utilization pathway inhibit *T.***
202 ***muris* egg hatching**

203 To understand why *T. muris* eggs incubated with *ΔeutN E. coli* displayed the
204 greatest reduction in hatching, we first determined whether disrupting other parts of the
205 ethanolamine utilization pathway (Fig. 3A) led to similar outcomes. *E. coli* mutants

206 lacking enzymes in the pathway—*ΔeutB*, *ΔeutC*, *ΔeutD*, *ΔeutE*, and *ΔeutG*—facilitated
207 egg hatching at rates similar to WT *E. coli* (Fig. 3B). In contrast to these *eut* operon
208 genes, *eutN* encodes a subunit of a proteinaceous shell that enables the efficient
209 colocalization of the *eut* enzymes with their cofactors and substrates within a
210 microcompartment and prevents diffusion of pathway intermediates (Yeates et al.,
211 2010). It is possible that disruption of the microcompartment architecture allows the
212 release of a soluble toxic intermediate. Therefore, we tested whether transferring the
213 supernatant from *ΔeutN* culture was sufficient to inhibit the ability of WT *E. coli* to
214 mediate hatching (Fig. 3C). Although transferring culture supernatant from *ΔeutN*
215 grown in isolation had no effect, supernatant isolated from *ΔeutN* that had been
216 incubated with eggs ($\Delta eutN^{egg}$) reduced hatching mediated by WT *E. coli* (Fig. 3D). This
217 suggests that *ΔeutN* produces a soluble toxic factor in the presence of *T. muris*
218 embryonated eggs.
219 Acetaldehyde is a known intermediate of the ethanolamine utilization pathway
220 that can readily form irreversible adducts with proteins, changing their conformation and
221 function (Donohue et al., 1983; Sorrell and Tuma, 1987) . Additionally, deletion of *eutN*
222 in *Salmonella* resulted in the greatest increase in acetaldehyde volatility among all *eut*
223 operon mutants during the first hours of growth (Penrod and Roth, 2006). Using a
224 fluorogenic hydrazone transfer (DarkZone) system to label aldehydes (Yuen et al.,
225 2016), we detected elevated levels of aldehydes in the culture supernatant of $\Delta eutN^{egg}$,
226 but not in the culture supernatant of the complemented *ΔeutN* strain or when the mutant
227 was grown in the absence of eggs (Fig. 3E and S3A). Aldehyde levels were also
228 elevated in *ΔeutD* (Fig. 3E), the other *E. coli* mutant of this pathway identified by the *C.*

229 *elegans* screen, although the increase following egg incubation was not as striking as
230 for *⊿eutN*, potentially explaining why deletion of *eutD* did not inhibit hatching (Fig. 2B).
231 The eut operon transcriptional regulator in *E. coli*, *eutR*, is sensitive to the
232 chemical environment (Penrod and Roth, 2006). We hypothesized that *eutR* expression
233 may be altered in the presence of *T. muris* eggs, thus explaining why aldehyde levels
234 are increased when bacteria are co-incubated with eggs. We found that *eutR*
235 expression in WT *E. coli* and *⊿eutN* significantly increased following egg incubation
236 (Fig. S3B). As a control, increased *eutR* expression was detected from WT *E. coli*
237 grown in minimal medium supplemented with ethanolamine, consistent with previous
238 studies (Penrod and Roth, 2006; Rowley et al., 2020).
239 Next, we deleted the rate limiting enzyme of the ethanolamine utilization
240 pathway, *eutC*, in the *⊿eutN* background (*⊿eutN⊿eutC)* to prevent the formation of toxic
241 intermediates (Penrod and Roth, 2006; Roof and Roth, 1989). We found that aldehyde
242 levels of *⊿eutN⊿eutC*^{egg} were similar to that of WT *E. coli* and that *T. muris* egg
243 hatching was completely restored when the assay was performed with this double
244 mutant (Fig. 3E-F). We also found that pre-treatment of *⊿eutN*^{egg} supernatant with an
245 aldehyde scavenger N-acetyl cysteine completely abrogated its effects on WT *E. coli*
246 and restored hatching (S3C-D). Additionally, we found that supplementation of
247 acetaldehyde alone was sufficient to inhibit hatching elicited by WT *E. coli* in a
248 concentration-dependent manner and confirmed that bacteria viability was unaffected
249 (Fig. S3, E-F).
250

251 ***T. muris* reared in mice colonized with *E. coli* mutants exhibit defects in worm**
252 **morphology and fertility.**

253 *In vitro T. muris* egg hatching serves as a sensitive assay to investigate
254 nematode-bacteria interactions, but the role of intestinal bacteria in subsequent steps of
255 *Trichuris* development remains obscure because they are difficult to recreate outside
256 the mammalian host. Given that the *C. elegans* screen was focused on development of
257 the reproductive tract, we established a bacterial monocolonization mouse model to
258 investigate the role of bacterial *fabH*, *eutN*, and *eutD* in *T. muris* development and
259 reproduction (Fig. 4A). After we verified that each *E. coli* mutant colonized germ-free
260 mice to levels similar to WT *E. coli* (Fig. S4A), monocolonized mice were gavaged twice
261 with 100 eggs and sacrificed two weeks after the second gavage. *E. coli* colonization
262 and cecum length were confirmed to be similar across groups on the day of sacrifice (42
263 dpi) (Fig. S4, A-B).

264 We were able to recover adult worms from the cecum of mice monocolonized
265 with WT *E. coli* but not germ-free mice (Fig. S4C), consistent with previous observations
266 (White et al., 2018), indicating that our assay allows investigation of mechanisms by
267 which *E. coli* contributes to *T. muris* development in an intact host. Our experimental
268 setup in which mice receive high doses of embryonated eggs was designed to
269 overcome the potential reduced hatching efficiency that may occur in mice lacking a
270 complex microbiota. Therefore, as expected, we did not detect any differences in worm
271 burden when comparing mice colonized with WT *E. coli* versus *⊿fabH*, *⊿eutN*, and
272 *⊿eutD* strains (Fig. S4C). However, many of the *T. muris* recovered from mice colonized
273 with these mutants displayed a striking deformity characterized by shortened length

274 (Fig. 4, B-C; indicated by arrowheads). Although worms from WT *E. coli*-colonized mice
275 were exclusively long in length, mice colonized with *⊿fabH*, *⊿eutN*, and *⊿eutD E. coli*
276 produced a mixture of both long and short length worms, defined as < 1cm. The defect
277 was most severe in mice monocolonized with *⊿eutN* from which most worms recovered
278 were short. To investigate if the shortened length of *T. muris* resulted from mutant *E.*
279 *coli* colonization affecting the host, we examined T cell subsets that have been
280 previously established as key determinants of host susceptibility (Bancroft et al., 1994;
281 D'Elia et al., 2009). Flow cytometric comparison of mesenteric lymph node T cells from
282 mice colonized with WT or *⊿eutN E. coli* revealed no significant differences in T helper
283 type 1 (Th1), T helper type 2 (Th2), regulatory T (T reg) cells, or IFN-γ producing T cells
284 (Fig. S4D-G).

285 The average number of freshly laid eggs per worm was not significantly different
286 between the conditions or when comparing long versus short worms (Figure S4H).
287 However, in stark contrast to worms from WT *E. coli*-colonized mice, which laid eggs of
288 the typical ovoid structure, worms harvested from mice colonized with *⊿fabH*, *⊿eutD*,
289 and *⊿eutN E. coli* laid more eggs that displayed an aberrant rounded morphology, and
290 in some cases lacked opercula and a distinct shell, and the inner contents were
291 disorganized (Fig. 4, D-E). These structurally aberrant eggs took longer to reach
292 embryonated morphology, and even after a prolonged incubation period, significantly
293 fewer eggs appeared embryonated in the *⊿eutN* and *⊿eutD* groups (Fig. 4F). Eggs laid
294 by worms from all three mutant-colonized groups of mice had significantly lower
295 hatching rates compared to eggs laid by worms from WT *E. coli*-colonized mice when
296 tested for bacteria-mediated hatching *in vitro* (Fig. 4G). These hatching defects

297 persisted even when eggs were allowed to embryonate twice the embryonation time
298 published in the literature for *T. muris* (Fig. S4I), suggesting disrupted and not delayed
299 development. In line with our *in vitro* data (Fig. 3F), monocolonization of mice with
300 *⊿eutN⊿eutC* abrogated the length and egg fitness defects of *T. muris* observed in
301 *⊿eutN*-colonized mice (Fig. 4, H-L). A similar rescue was seen when mice were
302 monocolonized with the *⊿eutN* complemented strain (Fig S4, J-L). These findings
303 indicating that bacterial deficiencies decrease *T. muris* worm size and egg fitness is
304 consistent with recent evidence showing that another parasitic nematode
305 *Heligmosomoides polygyrus*, lays fewer eggs and exhibits similar length defects when
306 reared in a germ-free host (Rausch et al., 2018).
307 To gain insight into the cause of morphologic and reproductive aberrancies in *T.*
308 *muris*, we performed RNA-Seq analysis of individual female worms (Fig S4M, Table
309 S2). The transcriptomes of worms harvested from WT *E. coli*-colonized mice clustered
310 separately from those of short and long worms harvested from mutant-colonized mice.
311 The latter did not segregate further according to length, representing no detectable
312 significant differences between short and long worms particularly in developmental
313 genes. Analysis of the top 50 most differentially detected genes between the WT- and
314 mutant-associated worms (Table S3) included genes related to *C. elegans* genes *egg-3*,
315 *egg-4*, *egg-5*, *alg-3*, and *alg-4* all of which are expressed in the germ line of *C. elegans*
316 and whose biological functions include roles in oogenesis, spermatogenesis,
317 fertilization, the egg-to-oocyte transition, and egg shell deposition (Boeck et al., 2016;
318 Cheng et al., 2009; Conine et al., 2010; Maruyama et al., 2007; Parry et al., 2009).
319 Crosschecking our 50 genes with published lifestage- and sex-specific transcriptomics

320 of *T. muris* (Foth et al., 2014), all genes found to be highly expressed in the female
321 worms from mutant-colonized mice were previously detected as upregulated in adults
322 (vs. larvae), providing additional evidence that the short worms are not disrupted in
323 somatic development. Additionally, these same genes were also previously detected as
324 more highly expressed in *T. muris* males compared to females (Foth et al., 2014).
325 Conversely, all but one of the genes that were downregulated in the worms from
326 mutant-colonized mice were found to be upregulated in *T. muris* females. These
327 discordances provide evidence of sexual development dysregulation in worms
328 harvested from mutant-colonized mice.

329 In conclusion, these results provide evidence for a previously undescribed role
330 for byproducts of microbial metabolism on nematode development, a role that appears
331 evolutionarily conserved. Despite lacking many genes specific to parasitism, our
332 findings support the utility of *C. elegans* as a model for bacteria-nematode interactions
333 because of its high sensitivity to its bacterial milieu. In addition to identifying two critical
334 pathways in bacteria, fatty acid biosynthesis and ethanolamine utilization, our findings
335 describe a novel pipeline that leverages genetic tools available in *C. elegans* to discover
336 new helminth biology. An important future direction would be to determine the role of
337 microbial byproducts in the setting of a complex microbiota. For instance, microbiota
338 rich in bacteria with highly active arginine biosynthesis or another pathway favorable for
339 *T. muris* reproduction may confer greater susceptibility to infection. Identifying the
340 microbes and their products that affect different stages of the helminth life cycle would
341 allow predictions and testable hypotheses regarding the impact of interindividual
342 differences in microbiota composition. We propose that *C. elegans* can be used as a

system for investigating the effects of specific microbial genes and pathways in supporting the parasitic nematode life cycle and aid in further understanding the transkingdom interactions that sustain human disease.

Acknowledgements

We wish to thank D. Jones, R. Rose, and L. Ash from the NYULH Metabolomics Laboratory (SCR_017935) and C. Yun, S. Cook, and D. Kahler from the High Throughput Biology Core (now Microscopy Laboratory, NIH S10 RR023704) for their help in acquiring and analyzing the data presented. Both Core Laboratories are funded partially by NIH/NCI P30CA016087. Some strains were built using strains provided by the CGC which is funded by the NIH Office Research Infrastructure Programs (P40 OD010440), and we thank WormBase. We also thank H. Darwin and M. Pacold for advice on microbial metabolism; S. Marion, C. Linton, M. Xu, A. Niranjan, D. Stokes, M. Lopez-Redondo, I. Irnov, V. Torres, S. Dyzenhaus, M. Hui, J. Richards (NYU), and E. Tait-Wojno (Univ. of Washington) for technical assistance and reagents; members of the Hubbard Lab, Cadwell Lab, and NYU Medical Scientist Training Program for constructive comments and technical assistance; and M. Alva, J. Carrasquillo, and D. Basnight for assistance with gnotobiotics.

Funding

NIH grant DK093668 (K.C.)
NIH grant AI121244 (K.C.)
NIH grant HL123340 (K.C.)
NIH grant AI130945 (K.C.)
NIH grant AI140754 (K.C.)
NIH grant DK124336 (K.C.)
NIH grant R01GM130152 (E.J.A.H.)
NIH grant R35GM134876 (E.J.A.H.)
NIH grant R01GM035769 (J.G.B.)
NIH grant 5T32AI100853 (M.V.)

NIH grant T32GM136573 (M.V.)
NIH grant T32GM007308 (M.V.)
Faculty Scholar grant from the Howard Hughes Medical Institute (K.C.)
Crohn's & Colitis Foundation (K.C.)
Kenneth Rainin Foundation (K.C.)
Judith & Stewart Colton Center of Autoimmunity (K.C.)
US National Cancer Institute (CA217809) (E.T.K.)
K.C. is a Burroughs Wellcome Fund Investigator in the Pathogenesis of Infectious Diseases.

Author contributions

M.V., R.D., E.J.A.H, and K.C. conceived the study and designed the experiments. M.V., R.D., and J.B. performed, analyzed, and interpreted all the experiments for *T. muris* and *C. elegans*. D.J.L. performed the bacterial cloning. H.S.P and E.T.K provided DarkZone and technical advice. J.C.D. provided technical assistance and advice for RNA sequencing and analysis. K.C., E.J.A.H, and J.G.B oversaw analysis and interpretation of all experiments described. M.V., R.D., E.J.A.H., and K.C. wrote the manuscript with inputs from all authors.

Competing interests

K.C. has received research support from Pfizer, Takeda, Pacific Biosciences, Genentech, and Abbvie. K.C. has consulted for or received honoraria from Puretech Health, Genentech, and Abbvie. K.C. holds U.S. patent 10,722,600 and provisional patent 62/935,035 and 63/157,225, and E.J.A.H. holds US patent 6,087,153.

Data and materials availability

All data needed to evaluate the conclusions in this study are available in the main text and the supplementary materials or available from the corresponding authors upon request.

Supplementary Materials

Methods

Figs. S1 to S4

Tables S1-S7

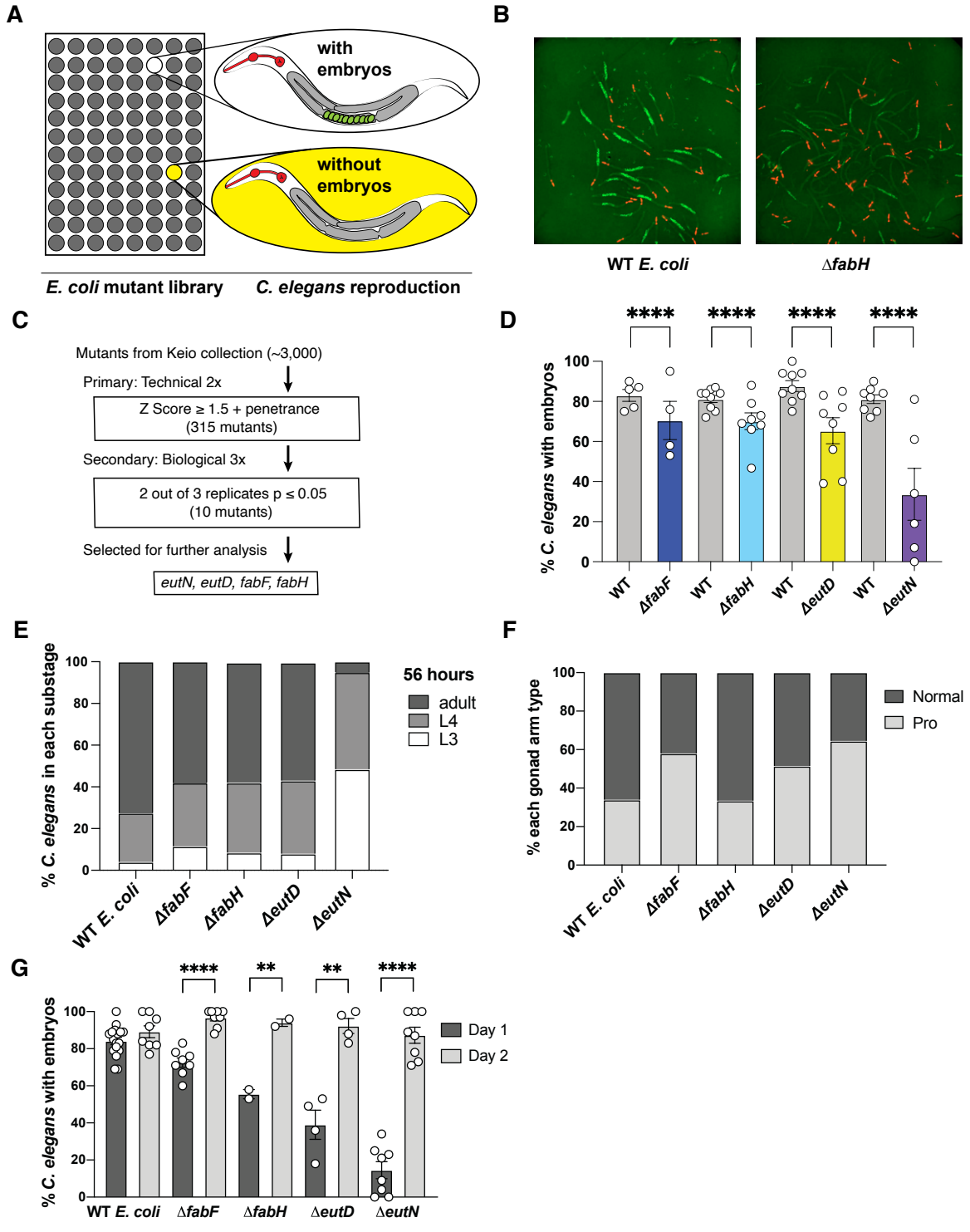

Fig. 1 Identification of *E. coli* mutants that delay *C. elegans* fertility. (A) Concept of high throughput screening of *C. elegans* raised on *E. coli* mutants from the Keio library.

(B) Example of reduced penetrance of *C. elegans* bearing embryos at a single time point; embryos marked with GFP and pharynx with mCherry. **(C)** Detailed flowchart for schematic in (A). **(D)** Percentage of *C. elegans* bearing embryos in replicates of four *E. coli* mutants of interest from the screen. Fisher's exact test for each mutant versus controls from the same plates; total n number of worms scored are (left to right): 913, 411, 1253, 583, 1643, 550, 1561, 232. **(E)** Somatic development is delayed in *C. elegans* raised on *⊿eutN*. Percent of worms at indicated stage at 56 hours after L1 seeding to wells containing the control or mutant bacteria. n ≥ 38 worms were scored for each *E. coli* mutant. *⊿eutN* is the only mutant that is statistically significantly different from the control GC1547 ($p \leq 0.001$). n number of worms scored (left to right): 52, 59, 61, 40, 54. **(F)** *⊿eutN* and *⊿fabF* delay germline development relative to somatic development. Percent of gonad arms displaying characteristic Pro phenotype. $p \leq 0.001$ for *⊿eutN* and *⊿fabF*. Pooled from two independent trials; n number of worms scored are (left to right): 87, 103, 79, 41, 61. **(G)** Fertility is delayed. Percent of worms with embryos on Day 1 and Day 2. $p \geq 0.05$ (not significant) for any mutant versus the control on Day 2. n number of worms scored (left to right): 547, 297, 242, 242, 60, 46, 124, 121, 253, 261. (D-G) Circles represent mean of independent biological replicates and bars show mean and SEM; pairwise Fisher's exact test versus controls (D-F) or Day 1 versus Day 2 (G). ** $p < 0.01$, **** $p < 0.0001$.

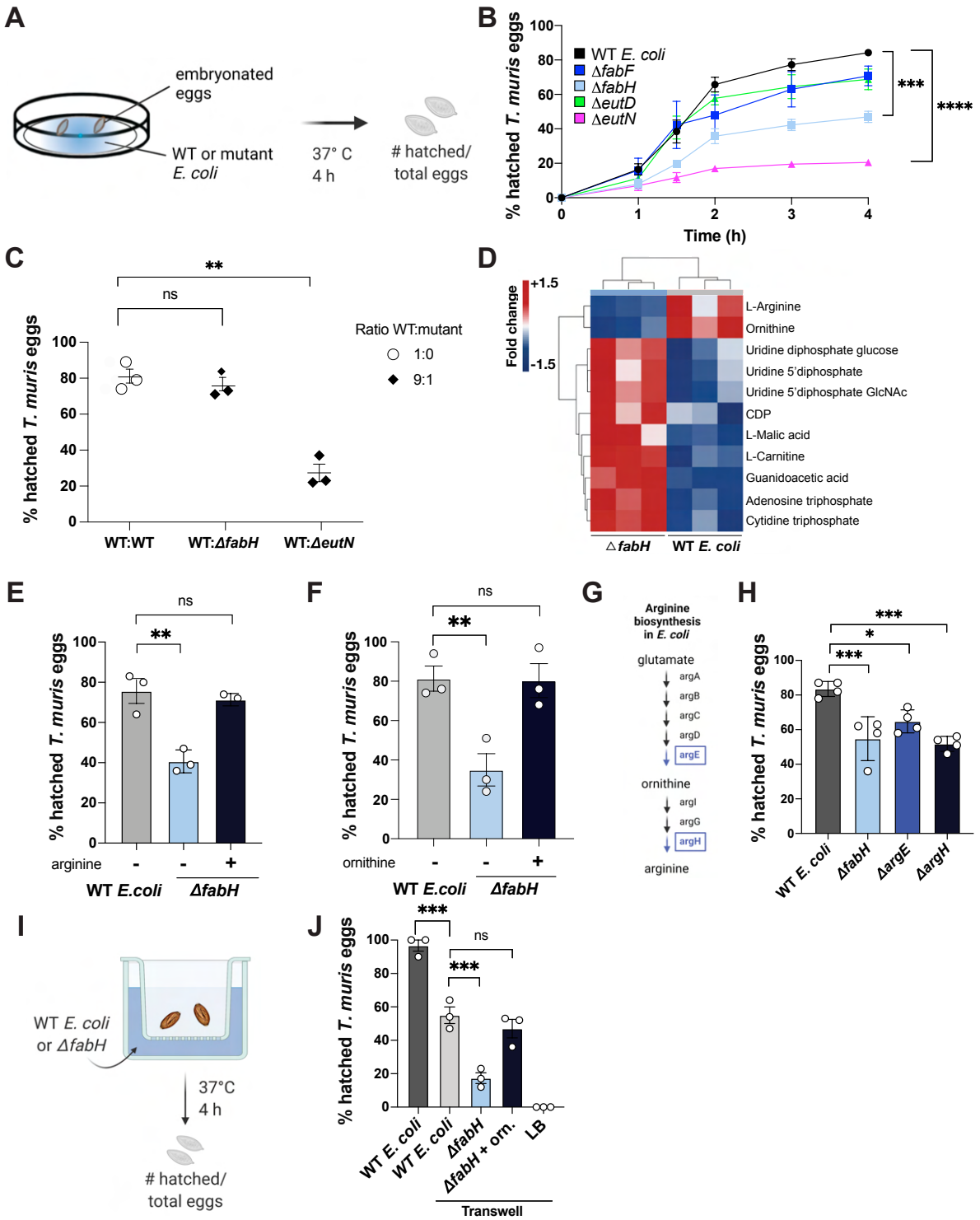

Fig. 2 *E. coli* mutants with altered metabolic byproducts delay *C. elegans* fertility and inhibit *T. muris* egg hatching. (A) Experimental approach for *in vitro* hatching assay. **(B)** Percent *in vitro* hatched *T. muris* eggs after incubation with overnight

433 cultures of four *E. coli* mutants identified from the *C. elegans* screen or WT *E. coli*.
434 Hatched eggs were checked using light microscopy at timepoints indicated (n = 4); h =
435 hours. **(C)** Hatching rates for mixtures of WT *E. coli* and WT *E. coli* or either Δ*fabH* or
436 Δ*eutN* overnight cultures in the ratios indicated. Total concentration of each mixture was
437 maintained at 1x 10^8 CFU/mL (n = 3). **(D)** Hierarchical clustering of metabolites that
438 were significantly ($p < 0.05$, Student's t-test) downregulated (blue) or upregulated (red)
439 in Δ*fabH* relative to WT. **(E, F)** Percent *in vitro* hatched *T. muris* eggs elicited by Δ*fabH*
440 and cultures supplemented with (E) 500μM arginine or (F) 100μM ornithine where
441 indicated (n=3). **(G)** Arginine biosynthesis pathway in *E. coli*. **(H)** Hatching rates elicited
442 by Δ*argE* and Δ*argH* (n = 4). **(I)** Experimental approach for hatching assay in a transwell
443 system. **(J)** Hatching quantified for eggs contained within a transwell chamber
444 separated from bacterial culture in the outer chamber by a membrane with 0.4μm pores.
445 Samples supplemented with ornithine as in (H) are indicated (n = 3). (B) One-way
446 analysis of variance (ANOVA) of area under curve compared to WT. (C, E-F, H, J) One-
447 way analysis of variance (ANOVA) with Dunnett's post-test compared to WT. For all
448 panels, measurements were taken from distinct samples. Graphs show means and
449 SEM. * $p < 0.05$, ** $p < 0.01$, *** $p < 0.001$, **** $p < 0.0001$. ns = not significant.
450

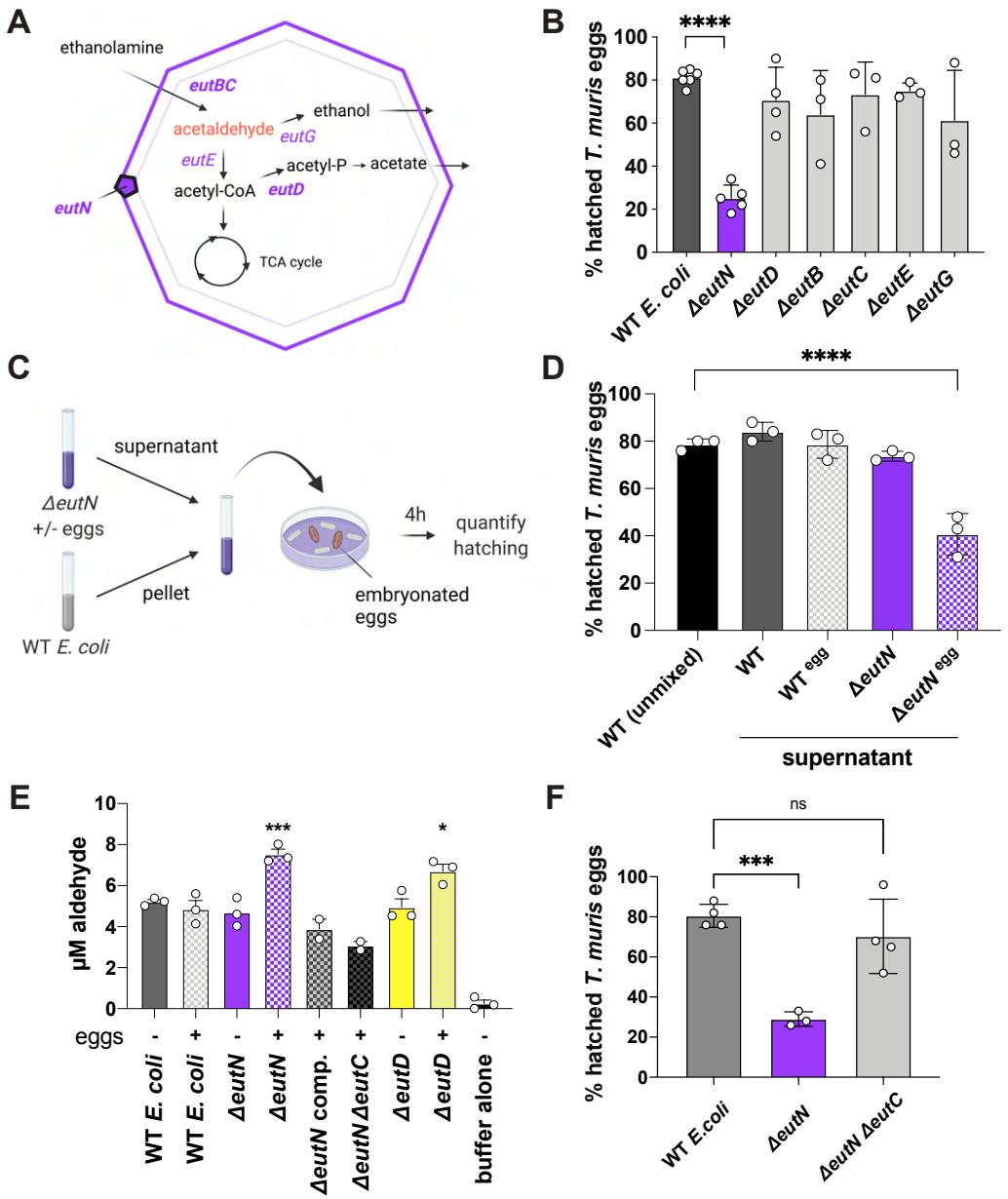

Fig. 3 Toxic intermediates of the *E. coli* ethanolamine utilization pathway inhibit *T. muris* egg hatching. (A) Ethanolamine utilization pathway in *E. coli*. Modified from (Kaval and Garsin, 2018). **(B)** Hatching rates for *eut* mutants in the Keio library and WT controls (n = 3-6). **(C)** Experimental approach to assess the toxicity of soluble factors produced by *E. coli* Δ*eutN*. Filtered supernatant from Δ*eutN E. coli* or controls grown with or without *T. muris* eggs for four hours were transferred to a dish containing WT *E. coli* and *T. muris* eggs. The ability of WT *E. coli* to mediate egg hatching in the presence

459 of supernatant was examined four hours later. **(D)** Quantification of hatching rates for
460 mixtures containing WT *E. coli* cells and the indicated filtered supernatants (n = 3). **(E)**
461 Aldehyde concentrations in supernatants of indicated *E. coli* strains incubated with or
462 without *T. muris* eggs; Δ*eutN* comp. = Δ*eutN* strain where *eutN* has been complemented
463 on a plasmid. **(F)** Hatching rates for Δ*eutN*Δ*eutC* double mutant (n = 4). (B, D-F)
464 Measurements were taken from distinct samples. The average per independent
465 experiment for at least three technical replicates shown. Graphs show means and SEM.
466 One-way analysis of variance (ANOVA) with Dunnett's post-test compared to WT. * $p <$
467 0.05, *** $p < 0.001$, **** $p < 0.0001$. ns = not significant.

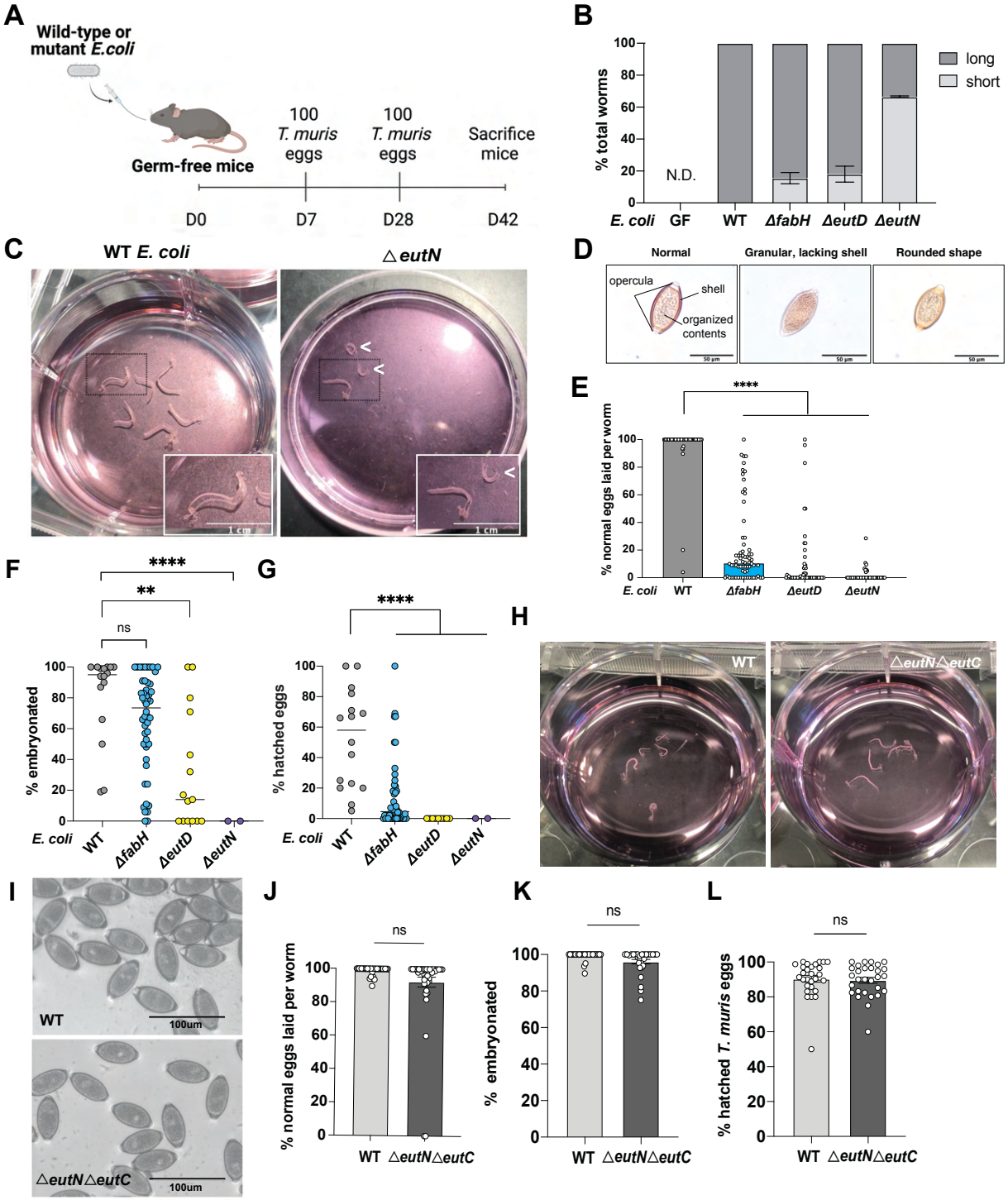

Fig. 4 *T. muris* reared in mice colonized with *E. coli* mutants exhibit defects in worm morphology and fertility. (A) Experimental approach for *T. muris* infection of mice monocolonized with WT or mutant *E. coli*. **(B)** Proportion of short and long worms harvested per mouse colonized by indicated *E. coli* strains; N.D. = not detected (n = 6-9

473 mice per group). **(C)** Representative images of worms harvested from mice
474 monocolonized with WT or *ΔeutN E. coli*. A representative short worm (indicated by
475 arrowhead) next to a long worm is shown in the inset for *ΔeutN E. coli*. **(D)**
476 Representative images of eggs laid by worms from (B). Worms were incubated in RPMI
477 medium overnight to trigger egg laying. **(E)** Proportion of total eggs laid per worm with
478 normal morphology. Circles represent individual worms (WT, n = 46; *ΔfabH*, n = 68;
479 *ΔeutD*, n = 58; *ΔeutN*, n = 50). **(F)** Percentage of embryonated eggs following 8-week
480 incubation. **(G)** Percentage of eggs in (F) that hatched after incubation with WT *E. coli*
481 for 4 hours at 37°C. **(H)** Representative photos of worms harvested from WT and
482 *ΔeutNΔeutC* monocolonized C57BL/6 mice. **(I)** Representative images of eggs laid by
483 worms harvested from monocolonized mice groups indicated**. (J)** Proportion of total
484 eggs laid per worm with normal morphology**. (K)** Percentage of embryonated eggs
485 following 8-week incubation. **(L)** Percentage of eggs in (K) that hatched after incubation
486 with WT *E. coli* for 4 hours at 37°C. (B, E, F-G) Graphs show (B) means and SEM or (E-
487 G) medians. One-way analysis of variance (ANOVA) with Dunnett's post-test compared
488 to WT. (J-L) Graphs show means and SEM. Two-tailed, unpaired t-test. For all panels,
489 measurements were taken from distinct samples. Data shown are pooled from two
490 independent experiments. ** $p < 0.01$, **** $p < 0.0001$. ns = not significant.

Methods

Keio Library growth and culture

The frozen Keio collection was stamped out onto 150mm LB kanamycin (30µg/ml) plates and grown overnight at 37°C. For *C. elegans* experiments, individual colonies were inoculated into 700 µl of LB-Kan (30µg/ml) in 96 deep well plates using a compatible pin replicator. The plates were sealed with pure link air porous tape (Invitrogen cat no. 12262010) and incubated for 16-18 hours at 37°C, shaking at 250 rpm. Cultures were diluted 10X in S-media in 96 well format and OD at 600 nm was recorded for future reference to ensure that candidate positive mutants grew to an OD similar to the GC1547 wild-type control wells in the same plate. (This was done since poor bacterial growth can reduce the percentage of gravid *C. elegans*; all 315 candidates from the primary screen passed this control). Bacterial cultures were pelleted by centrifugation at 2000 rpm for 30 minutes. Supernatant was discarded and the pellet was resuspended in 100µl of S-media. 40µl of the culture was transferred into two separate plates (two technical replicates; black-walled, clear bottom 96-well microplates; Corning Cat. No. 3904) using a multi-channel pipette. The GC1547 control wild-type strain was a kanamycin resistant transformant of the Keio library starting strain BW25113, carrying the pET28a plasmid. For *T. muris in vitro* hatching assays, *E. coli* was grown overnight for 12-14 hours in Luria-Bertani broth with shaking at 225 rpm at 37 °C.

Primary screen

C. elegans GC1474 (Table S1; derived by outcrossing GC1373 (Roy et al., 2018) of the genotype *glp-1(e2141); end-1::gfp; myo-2p::mCherry*) was maintained on OP50 *E. coli* on NGM plates at 20ºC and synchronized in the L1 larval stage using hypochlorite treatment followed by overnight hatching in egg buffer (Shaham, 2006). 40-50 L1 larvae were seeded into 96-well plates in technical duplicate with 40µl of *E. coli* mutant cultures and incubated at 20°C with mild shaking in a humidified chamber for 62-65

hours. At this timepoint, control worms were fully gravid adults; control GC1547 bacteria were included on each plate in wells void of library bacteria. Prior to imaging, 40µl of 2mM levamisole was added to each well to immobilize the worms. The plates were then sealed with aluminum foil (Corning Cat. No. 6570) and imaged to detect both green (embryos) and red (pharynx) fluorescent markers using arrayscan (Thermo Scientific VTI). Images were captured at 2.5X magnification 2x2 binning in a 16 mm^2 field and digitally archived. Images captured on the red and green channels were merged in ImageJ using macros written to automate the process. Each adult animal was scored visually as “with embryos” (green embryos visible in the uterus) or “without embryos” (no green embryos visible in the uterus), and the number of worms without embryos and the total number of worms (excluding any that were arrested or any that crossed the edge of the well). Wells in which many animals had not reached adulthood were marked and were not considered further in our analysis. Ten such bacterial mutants grew well by OD but did not support worm development.

Additional culling of potential hits was performed. A variety of technical factors eliminated fewer than 10% of the total: 54 library wells were devoid of bacteria as per the plate map; 58 had a gene name in the library but the bacteria did not grow (either on solid or liquid culture); 41 were missed due to human error while scoring (noted as largely fertile but not counted individually); 5 had low n; 4 were not included due to reasons classified as ‘other’ (e.g., poor image) and 10 wells had poor worm growth in both replicates.

Worm counts (with/without embryos) were exported into ActivityBase (IDBS, https://www.idbs.com; a Scientific informatics software platform) and the robust Z score (a statistical measure that takes into account the median plate “without embryos” percent) was calculated for every well to minimize problems associated with plate to plate variation. Each well was analyzed with respect to percent worms without embryos, consistency (across technical replicates) and robust Z score. A cut-off of robust $Z \geq 1.5$ was selected as “Z positive” (≤ 10% of the wells per plate scored above this threshold).

We also calculated the penetrance of worms without embryos for pooled technical replicates.

Criteria for selection in the primary screen weighed the robust Z and penetrance, with special consideration for cases where only one replicate was available. We included those wells for which only one technical replicate was available provided that well made the RobZ cut off (≥ 1.5) and/or percent non-gravid worms as further described below. Reasons for single-replicate included low n (62 wells), human error (49 wells), worm arrest (31 wells), poor image quality (22 wells) and 1 well marked as 'other'. Considering Z score, penetrance and replicates, the candidates were further classified as follows: High, A: both replicates Z positive and average penetrance of non-gravid worms > 20%, or B: one replicate available and it is Z positive and > 20%, or C: both replicates available but only one is Z positive and non-gravid ≥ 30%. Medium, A: both replicates Z positive and pooled non-gravid percent 13-20%, or B: only one replicate available which is Z positive and 13-20% penetrance of worms without embryos, or C: both replicates available but only one is Z positive with pooled non-gravid penetrance between 20-30%. Low: both replicates available, but only one is Z positive and non-gravid percent between 12.5-20%. This analysis yielded 315 primary screen candidates.

We then plotted the percent non-gravid in descending order for every well per plate and noted the inflection point (see (Roy et al., 2018)). We placed a subset of the mutants that passed the criteria above onto these plots and observed a strong correlation: wells with larger Z scores all appeared above the inflection point.

Secondary screen: reproducibility

The 315 candidates from the primary screen were re-selected from the original Keio library and gridded onto secondary screen plates. Two plates included only high priority candidates or a combination of randomly selected high, medium and low priority candidates to help assess whether there was a correlation between penetrance and reproducibility. No such correlation emerged, but these plates were considered as additional replicates in the analysis going forward (hence 6 plates) though 315 mutants.

Control bacteria were included in all secondary screen plates. Three biological replicates were performed in technical triplicate and scored and analyzed as described above. Technical replicate non-gravid/gravid counts were pooled and analyzed in pairwise comparison with the control on the same plates using Fisher's exact test. Candidates with p-values ≤ 0.05 in at least 2 out of 3 biological replicates were chosen for further analysis. This analysis yielded 10 candidates.

PCR validation of selected Keio mutants (completed for all ten hits)

We amplified and sequenced PCR fragments ~150 bp upstream and downstream of the predicted gene from each mutant and the control. Nested primers were used to sequence the PCR fragment and confirm the presence of the FRT and kanamycin cassette in the mutant DNA (Tables S3, S5).

P1 transduction

Mutant alleles comprising a kanamycin-resistance marker within a gene deletion were introduced into BW25113 by P1 transduction (Thomason et al., 2007) from the Keio collection (Baba et al., 2006) .The kanamycin-resistance cassette was subsequently excised to generate a markerless in-frame gene deletion by transformation with the temperature-sensitive plasmid pCP20 (Cherepanov and Wackernagel, 1995), which encodes FLP recombinase, and growth at 30°C. Finally, pCP20 was eliminated from the cells by growth at 42°C.

Complementation

For *fabH* and *eutN*, the bacterial gene coding regions plus 20 bp upstream were inserted into pBR322 downstream of a plasmid promoter by Gibson Assembly. The wild-type genomic DNA was amplified and assembled with a PCR fragment obtained from the pBR322 vector (specific primers are listed in Table S5; the fragment excluded part of the Amp^R gene between *Eco*RI and *Pst*I restriction site). PCR products were

purified using gel extraction kit (QIAEX II cat no. 20021) and 100 ng of vector was used in 1:1 molar reaction with the genomic fragment. The assembly reaction was then transformed into high efficiency DH5alpha cells (NEB C2987I). For *eutD*, the protein-coding region was amplified by PCR and cloned between the NdeI and XbaI sites downstream of the *lac*UV5 promoter of plasmid pPlacRppH6 so as to replace the *rppH* coding region (Deana et al., 2008). Plasmid preparations (Qiagen mini prep kit Cat no.27106) were sequenced using plasmid-specific primers (Table S5). Plasmids were confirmed by DNA sequence and transformed into the respective mutant (so as to create strains GC1558, GC1559, and GC1650 for *eutN* rescue, *fabH* rescue, and *eutD* rescue, respectively) and tested for reduced penetrance of the *C. elegans* non-gravid phenotype upon feeding.

Developmental timing and germline analysis

Somatic development assay

C. elegans were maintained on OP50, synchronized by hypochlorite treatment and allowed to hatch at 20ºC with shaking. 30-40 L1 larvae were seeded in 96 deep well plates with each well carrying a specific mutant clone. Worms were incubated at 20ºC with shaking for 48 hours and monitored at 400X on a Zeiss Z1 Axio Imager for vulval morphology (Mok et al., 2015) at specific time points.

Pro phenotype assay

glp-1(ar202) animals were scored for the Pro phenotype upon feeding with mutant bacteria using the same strategy as for the primary screen. Worms were maintained at 15ºC on OP50 synchronized and grown in 96 deep well format as above. Day 1 (~72 hours post seeding) worms were fixed and DAPI stained and each gonad arm was scored for the Pro phenotype (Pepper et al., 2003) at 400X.

Fertility at Day 2

GC1474 worms were maintained at 20ºC on OP50, synchronized as L1 larvae and grown in 96 deep well format as above. Worms were anesthetized and imaged as in the screen on Day 1 and Day 2 to determine changes in penetrance of fertile worms.

Progenitor zone nuclei counts at L4-Adult molt

Worms grown on GC1547 control, *eutN*, *eutD,* and *fabH* mutant bacteria were monitored for vulval development and isolated at the L4-adult molt. Worms were then stained with DAPI (Michaelson et al., 2010) and 0.5µm Z-stack images were collected and analyzed using ImageJ to determine the number of germ cells in the PZ. In approximately 30% of the worms, the transition zone was not clear. These were censored from the analysis.

Assay for dependence on DAF-7/TGFß and DAF-2 IIS pathways

C. elegans strains GC1474, GC1545 and GC1250 (Table S2) were hypochlorite-synchronized and hatched overnight at 20ºC. L1 larvae were seeded into 96 deep well plates containing specific bacterial mutants and scored for the presence of embryos in adults on Day 1 on Zeiss compound microscope at 100X.

Parasite maintenance

Stock eggs of *T. muris* E strain (Ramanan et al., 2016) were maintained in the NOD.Cg-*Prkdc*^{scid}/J (Jax) mouse strain in a specific pathogen free (SPF) facility and propagated as previously described (Antignano et al., 2011). Each egg batch was confirmed to hatch at ≥ 80% *in vitro* using method below and WT *E. coli* before use in subsequent experiments.

***In vitro* hatching of *T. muris* eggs**

T. muris eggs were hatched *in vitro* by mixing 25µL of embryonated eggs at a concentration of 1 egg/1µL suspended in sterile water with 10µL of *E. coli* overnight culture and 15µL sterile LB in individual wells of a 48 well plate. Plates were incubated

at 37°C and checked every hour for a total of four hours on the Zeiss Primovert microscope to enumerate hatched eggs. Rates describe hatching after four hours of incubation unless otherwise indicated. Experiments utilizing transwell inserts (Millicell) were performed as previously described (Koyama, 2016). For experiments where cell-free supernatant was used, supernatant and cells were isolated by centrifugation and filtration through a 0.22µm syringe filter or after wash with autoclaved ddH20, respectively. Incubation with embryonated eggs was performed by mixing *T. muris* eggs at a concentration of 15 eggs/2 mL culture and keeping at 37°C for four hours.

Metabolomics

Sample preparation

Individual colonies (obtained after streaking frozen bacteria onto LB-kanamycin plates and incubating at 37ºC) were inoculated in 30 ml of LB-kanamycin (30µg/ml) liquid in a 50ml falcon tube. Cultures were grown for 16-18hr at 37ºC with 250 rpm shaking and then bacteria were pelleted by centrifugation at 1500 rpm for 20-30 minutes at 4ºC. The supernatant was transferred to a fresh tube, filtered through 0.2µm filter (Corning (431229) and frozen at -80ºC for future analysis. Pellets were resuspended in 7.5 ml of S-media (for ~250ml of S-media the recipe was 240ml of S-basal, 2.5ml of 1M potassium citrate- final concentration of 10mM, 2.5ml of 1M trace metals for final concentration of 10mM, 750µl of 1M $MgS0_4$ for final concentration of 3mM, 750µl of 1M $CaCl_2$ for final concentration of 3mM, 72µl of 100mg/ml of kanamycin for final concentration of 30µg/ml). This solution was filter sterilized using a 500ml Nalgene filter (291-3320 Fisher). Post filter sterilization, 250µl of 5mg/ml cholesterol – final concentration of 5µg/ml and 2.5ml of 250µg/ml fungizone for final concentration of 2.5µg/ml (BP264550 Fisher).

The number of CFU/ml was estimated for each culture by plating dilutions (10µl of culture was mixed with 900µl of S-media to get 10^2 or 1:100 dilution, which was then serially diluted to 1:10^5 or 1:10^6 on LB agar plates and counting colonies after growth at 37°C. The remaining culture was incubated at 20ºC with mild shaking overnight to

mimic *C. elegans* growth conditions. Based on CFU/ml measurements, 10^{10} cells were fast filtered (EZFIT Vacuum Manifold, Millipore EZFITLOW03 with Microfil V, Millipore MVHAWG124) and metabolite extracts were isolated as previously described (Irnov et al., 2017). Three independent biological samples were extracted on three independent days and subsequently analyzed by the NYU Langone Metabolomics Core Resource Library.

LC-MS/MS with the hybrid metabolomics method

Samples were subjected to an LCMS analysis to detect and quantify known peaks. A metabolite extraction was carried out on each sample based on a previously described method (Pacold et al., 2016). The LC column was a Millipore™ ZIC-pHILIC (2.1 x150mm, 5µm) coupled to a Dionex Ultimate 3000™ system and the column oven temperature was set to 25°C for the gradient elution. A flow rate of 100µL/min was used with the following buffers: A) 10mM ammonium carbonate in water, pH 9.0, and B) neat acetonitrile. The gradient profile was as follows; 80-20%B (0-30 min), 20-80%B (30-31 min), 80-80%B (31-42 min). Injection volume was set to 2µL for all analyses (42 min total run time per injection).

MS analyses were carried out by coupling the LC system to a Thermo Q Exactive HF™ mass spectrometer operating in heated electrospray ionization mode (HESI). Method duration was 30 min with a polarity switching data-dependent Top 5 method for both positive and negative modes. Spray voltage for both positive and negative modes was 3.5kV and capillary temperature was set to 320°C with a sheath gas rate of 35, aux gas of 10, and max spray current of 100µA. The full MS scan for both polarities utilized 120,000 resolution with an AGC target of 3e6 and a maximum IT of 100ms, and the scan range was from 67-1000 *m*/*z*. Tandem MS spectra for both positive and negative mode used a resolution of 15,000, AGC target of 1e5, maximum IT of 50ms, isolation window of 0.4m/z, isolation offset of 0.1m/z, fixed first mass of 50m/z, and 3-way multiplexed normalized collision energies (nCE) of 10, 35, 80. The minimum AGC target was 1e4 with an intensity threshold of 2e5. All data were acquired in profile mode.

Hybrid Metabolomics Data Processing

Relative quantification of metabolites

The resulting Thermo™ RAW files were converted to mzXML format using ReAdW.exe version 4.3.1 to enable peak detection and quantification. The centroided data were searched using an in-house python script Mighty_skeleton version 0.0.2 and peak heights were extracted from the mzXML files based on a previously established library of metabolite retention times and accurate masses adapted from the Whitehead Institute (Chen et al., 2016), and verified with authentic standards and/or high resolution MS/MS spectral manually curated against the NIST14MS/MS (Simon-Manso et al., 2013) and METLIN (2017)(Smith et al., 2005) tandem mass spectral libraries. Metabolite peaks were extracted based on the theoretical *m*/*z* of the expected ion type e.g., $[M+H]^+$, with a ±5 part-per-million (ppm) tolerance, and a ± 7.5 second peak apex retention time tolerance within an initial retention time search window of ± 0.5 min across the study samples. The resulting data matrix of metabolite intensities for all samples and blank controls was processed with an in-house statistical pipeline Metabolyze version 1.0 and final peak detection was calculated based on a signal to noise ratio (S/N) of 3X compared to blank controls, with a floor of 10,000 (arbitrary units). For samples where the peak intensity was lower than the blank threshold, metabolites were annotated as not detected, and the threshold value was imputed for any statistical comparisons to enable an estimate of the fold change as applicable. The resulting blank corrected data matrix was then used for all group-wise comparisons, and t-tests were performed with the Python SciPy (1.1.0) (Virtanen et al., 2020) library to test for differences and generate statistics for downstream analyses. Any metabolite with p-value < 0.05 was considered significantly regulated (up or down). Heatmaps were generated with hierarchical clustering performed on the imputed matrix values utilizing the R library pheatmap (1.0.12) (Kolde, 2015). Volcano plots were generated utilizing the R library, Manhattanly (0.2.0). In order to adjust for significant covariate effects (as applicable) in the experimental design the R package, DESeq2 (1.24.0) (Love et al., 2014) was used to test for significant differences. Data processing for this correction

required the blank corrected matrix to be imputed with zeroes for non-detected values instead of the blank threshold to avoid false positives. This corrected matrix was then analyzed utilizing DESeq2 to calculate the adjusted p-value in the covariate model.

Arginine and ornithine supplementation assay

fabH mutant *E. coli* or wild-type control was grown with 500μM or 100μM ornithine in LB-kanamycin overnight at 37ºC with 250 rpm shaking. For *C. elegans* experiments, worms were imaged on Day 1 as described for the primary screen. For *T. muris* experiments, hatching assay was performed as described above.

DarkZone labeling of aldehydes

Cell-free supernatants isolated from *E. coli* overnight cultures were incubated with 20μM DarkZone dye pre-dissolved in DMSO, 5mM 2,4 dimethoxyaniline catalyst (TCI America) pre-dissolved in DMSO, and buffer (100mM Tris pH 6.8, 150 mM NaCl) in a 96 well optical flat-bottom plate (Thermo-Fisher) in duplicate at 37°C for 1 hour. Adhesive plate seals were used to prevent evaporation of aldehydes. Fluorescence was measured using an EnVision 2 103 Multi-label Reader (PerkinElmer). Duplicate measurements were averaged.

Quantitative PCR

Bacterial cells grown *in vitro* were pelleted and washed with RNA Protect (Qiagen) and PBS. For all samples, RNA was was isolated using the RNeasy micro kit with DNase treatment (Qiagen). Synthesis of cDNA was conducted with the High-Capacity cDNA Reverse Transcription Kit (Applied Biosystems). Samples were run without reverse transcriptase to control for genomic DNA contamination. Quantitative PCR was performed using SybrGreen (Roche) on a Roche480II Lightcycler using the following primers indicated in Table S5. Two technical replicates of each biological replicate were

included for each gene target. Relative expression of the respective genes to *16S* rRNA expression was calculated using the $\Delta\Delta C_T$ method.

N-acetyl cysteine supplementation assay

Bacterial cells and cell-free supernatants of WT *E. coli* and *eutN* mutant *E. coli* were isolated as described above. A 100mg/mL stock concentration of N-acetyl cysteine (Millipore Sigma) was dissolved in MilliQ water by stirring at 70°C. The N-acetyl cysteine was then added to supernatants at the concentrations of 8μM, 10 μM, 30 μM, and 50 μM and incubated at room temperature for one hour. WT *E. coli* cells were then resuspended in the supernatants and incubated with *T. muris* eggs to perform the hatching assay as described above.

Mice

Gnotobiotics

Previously described germ-free C57BL/6J mice (Martin et al., 2018) were maintained in flexible film isolators, and absence of faecal bacteria and fungi was confirmed by aerobic culture in brain heart infusion, sabaraud and nutrient broth (Sigma), and qPCR for bacterial 16S and eukaryotic 18S ribosomal RNA genes through sampling of stool from individual cages in each isolator on a monthly basis. Mice were transferred into individually ventilated Tecniplast ISOcages for infections to maintain sterility under positive air pressure. All animal studies were performed according to approved protocols and ethical guidelines established by the NYU Grossman School of Medicine Institutional Animal Care and Use Committee (IACUC) and Institutional Review Board.

Murine in vivo infections

Female mice were monocolonized at 6-8 weeks of age by oral gavage with 1×10^8 colony forming units per mL (CFU/mL) of indicated *E. coli* strains. Overnight *E. coli* cultures were diluted 1:100 in Luria-Bertani broth followed by 2-3 hours of growth until 1×10^8 CFU/mL was reached. Bacterial density was confirmed by dilution plating. Cultures were pelleted by centrifugation at 2437g for 10 minutes and washed once with

sterile 1x PBS. Pellets were then resuspended in sterile 1x PBS and mice were inoculated by oral gavage with $1x10^8$ CFU in a volume of 100µL. Inoculum was verified using dilution plating of aliquots.

7 and 28 days later, mice were infected by oral gavage with ~100 embryonated *T. muris* eggs. Individual worms were collected from cecal contents of all infected mice and washed in RPMI 1640 (Corning) supplemented with penicillin (100U/ml) and streptomycin (100µg/ml; Sigma). To evaluate egg laying, each worm was placed into individual wells of a 48 well plate with 200µL supplemented RPMI. Plates were then incubated at 37°C overnight in a closed tupperware (Sistema) lined with damp paper towels. The following day, eggs laid were enumerated using a Zeiss Primovert light microscope at 100X. Samples containing ~1000 eggs per condition were mounted on glass slides with glycerol mounting medium (Sigma-Aldrich) and analyzed using a Zeiss Axio Observer at 400X with oil emersion for color images or EVOS FL Auto (Life Technologies) at 200X for black and white images. Images were processed using ImageJ.

Flow Cytometry

Cells from mesenteric lymph nodes were isolated and stimulated as previously described (Ramanan et al., 2016). Stimulated cells were stained with anti-CD45 Pacific Blue, anti-CD3ε FITC, anti CD4 APC-Cy7, and anti-IFNγ AF700 from Biolegend and anti-CD19 PerCP Cy5.5 from eBioscience. Fixation and permeabilization buffers from Biolegend were used for intracellular cytokine staining, and a fixable live/dead stain from Biolegend was used to exclude dead cells. For nuclear staining, unstimulated cells were stained with anti-CD45 Pacific Blue, anti-CD3 FITC, anti-CD4 APC-Cy7, anti-FoxP3 PE-Cy7, and anti-Tbet APC from Biolegend, and anti-CD19 PerCP Cy5.5 and anti-GATA3 PE from eBioscience using the Foxp3 staining kit (eBioscience). Flow cytometric analysis was performed on a CytoFLEX analyzer (Beckman Coulter) and analyzed using FlowJo 10.0.8.

RNA isolation from harvested *T. muris* and RNA-seq

T. muris harvested from mice ceca were immediately transferred to RPMI 1640 (Invitrogen) supplemented with penicillin (100U/ml) and streptomycin (100µg/ml; Sigma) and stored at -80°C. RNA from individual worms was isolated using the RNeasy micro kit with DNase treatment (Qiagen). RNA-seq library preparation was done at the NYU School of Medicine Genome Technology Core using an automated Trio enrichment library preparation protocol (NuGEN). Libraries were then sequenced on a NovaSeq 6000 (Illumina). All sequences have been deposited at NCBI under the BioProject PRJNA803354.

RNA-seq analysis

Raw RNA-seq reads were trimmed using Trimmomatic v.036 (Bolger et al., 2014) and aligned to the reference *T. muris* genome (GenBank Assembly Accession: GCA_000612645.2) using the splice-aware STAR v2.7.3 (Dobin et al., 2013). The featureCounts command from Subread v1.6.3 (Liao et al., 2014) was used to generate counts for each gene based on how many aligned reads overlapped the exons of that gene. These counts were then normalized and used to test for differential expression using negative binomial generalized linear models implemented by DESeq2 v1.24.0 (Love et al., 2014).

Functional gene annotation of RNA-Seq hits

Annotation of the 50 most differentially detected hits from the RNA-seq analysis described above was performed using WormBase (version WS283) searches and BLAST searches against the *C. elegans* reference genome using WormBase BLAST/BLAT. The E-value threshold was set at 1E+0 and the *C. elegans* Sequencing Consortium genome project database was used. *C. elegans* genes with the highest homology were noted and their functional descriptions derived using WormBase WormMine. Stage- and sex-specific expression of hits were assigned based on previously published data (Foth et al., 201cl4).

Statistical analysis

Statistical tests and parameters used, including the definition of central value and the exact number (n) of mice or worms per group, are annotated in the corresponding figure legend. All analyses were performed with Graphpad Prism version 8.4.3 for Mac (GraphPad). The numbers of animals or biological replicates used herein were estimated on the basis of a power analysis with the following assumptions: the standard deviation will be roughly 20% of the mean; p values will be less than 0.05 when the null hypothesis is false; and the effect size (Cohen's d) is between 1.0 and 2.0. We have also carefully chosen the indicated sample size on the basis of empirical evidence of what is necessary to interpret the data and statistical significance.

Supplementary Figures

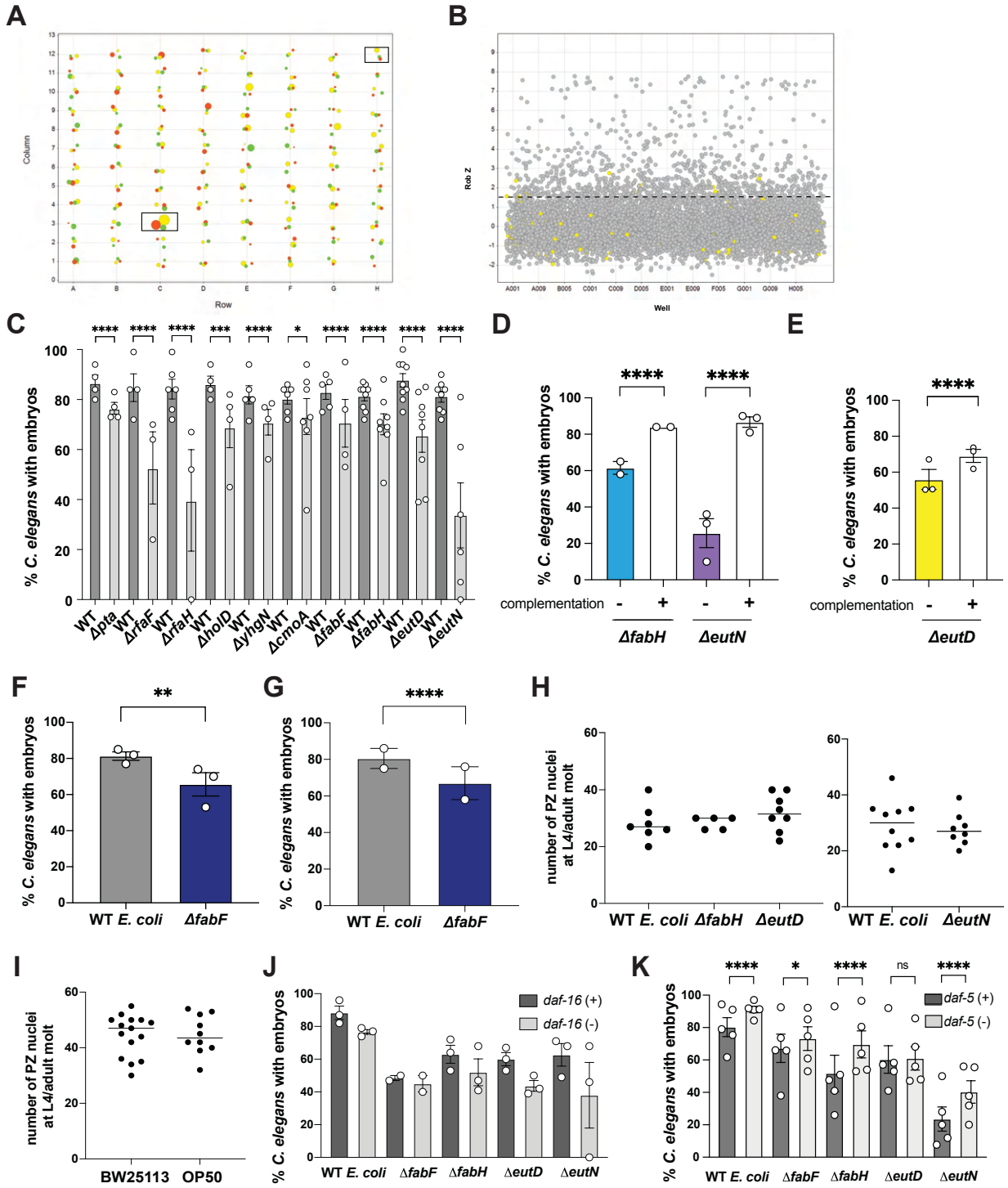

Fig. S1 Primary screen selection criteria, validation of *E. coli* mutants, and effect of mutant *E. coli* on *C. elegans*, related to Fig. 1. (A) Representative bubble plot from

secondary screen replicates. One of the six 96-well plates used in the secondary screen is shown here rendered using Vortex software data visualization tool. The size of the bubble represents percent of worms without embryos that is calculated from three technical replicates, while the color indicates the three biological trials. Boxed wells H12 and C3 indicate the negative control and a positive hit in two out of three replicates based on statistical tests**. (B)** Scatter plot showing the Robust Z (Rob Z) score for all primary screen wells scored. Scatter plot was generated using Vortex dotmatics software. Yellow dots indicate wells containing the negative control bacteria (GC1547). Dashed line indicates cut-off for Rob Z criterion. **(C)** Percentage of *C. elegans* bearing embryos in replicates of ten *E. coli* mutants identified from the secondary screen. Total n number of worms scored are (left to right): 505, 291, 418, 103, 879, 80, 586, 295, 474, 229, 1100, 501, 913, 411, 1253, 583, 1643, 550, 1561, 232. **(D)** Δ*eutN* and Δ*fabH* complementation suppresses *C. elegans* fertility defect. Total n number of worms scored is (left to right): 220, 197, 744, 1078. **(E)** Δ*eutD* complementation suppresses *C. elegans* fertility defect. Total n number of worms scored is 2276 (Δ*eutD*) and 2283 (Δ*eutD* with complementation). **(F, G)** Δ*fabF* phage transductant mimics *C. elegans* fertility defect of Δ*fabF* original clone. Circles represent mean of four independent biological replicates and bar is SEM. (F) Original *fabF* isolate from library (n = 330, 214 total worms scored, WT and Δ*fabF*, respectively), and (G) *fabF* transductant (n = 231, 66 total worms scored). **(H)** The number of progenitor zone nuclei of *glp-1(e2141)* at the L4 to Adult molt is not significantly different in worms raised on Δ*eutN*, Δ*fabH* or Δ*eutD* versus control *E. coli*. Scatter plots showing number of progenitor zone germ cell counts; each dot represents one gonad arm scored. We noted that in ~30% of *eutN* mutants (relative to 10% in control), the border of the PZ was difficult to detect; these were censored from PZ counts. The elevated penetrance of this phenotype in the Δ*eutN*-fed worms may represent a meiotic entry defect, accounting for the delay in germline development relative to somatic development. **(I)** No significant difference is observed between the number of progenitors in worms grown on BW25113 versus OP50 on standard NGM solid media. We note that the number of progenitors is markedly lower in the *glp-1(e2141)* mutant background after growth on liquid versus growth on solid media; the Keio starting strain was used in (H) since OP50 is sensitive

to kanamycin. **(J, K)** Fertility delay is not suppressed by loss of *daf-16,* nor is it unambiguously suppressed by loss of *daf-5*. Percent of worms with embryos on Day 1 in (J) *daf-16(+); daf-2(e1370) glp-1(e2141) or daf-16(m26); daf-2(e1370) glp-1(e2141)* and (K) *daf-5(+); glp-1(e2141) or daf-5(e1386); glp-1(e2141).* Loss of *daf-5* elevated the percentage of gravid worms on wild-type (WT) *E. coli*. Therefore, biological significance of a greater percentage of gravid *daf-5(e1386)* compared to *daf-5(+)* raised on the various mutant *E. coli* is unclear. Circles represent mean of independent biological replicates and bar is SEM. Total n number of worms scored are (left to right): **(J)** 269, 203, 207, 245, 179, 255, 229, 214, 200, 233 and (K) 460, 399, 386, 470, 379, 445, 388, 428, 554, 640. For (J), there is no significant suppression of the fertility delay in any case. Statistics: ANOVA and Student's t-test (H and I, respectively) and Fisher's Exact test (all other panels). * $p < 0.05$, ** $p < 0.01$, *** $p < 0.001$, **** $p < 0.0001$.

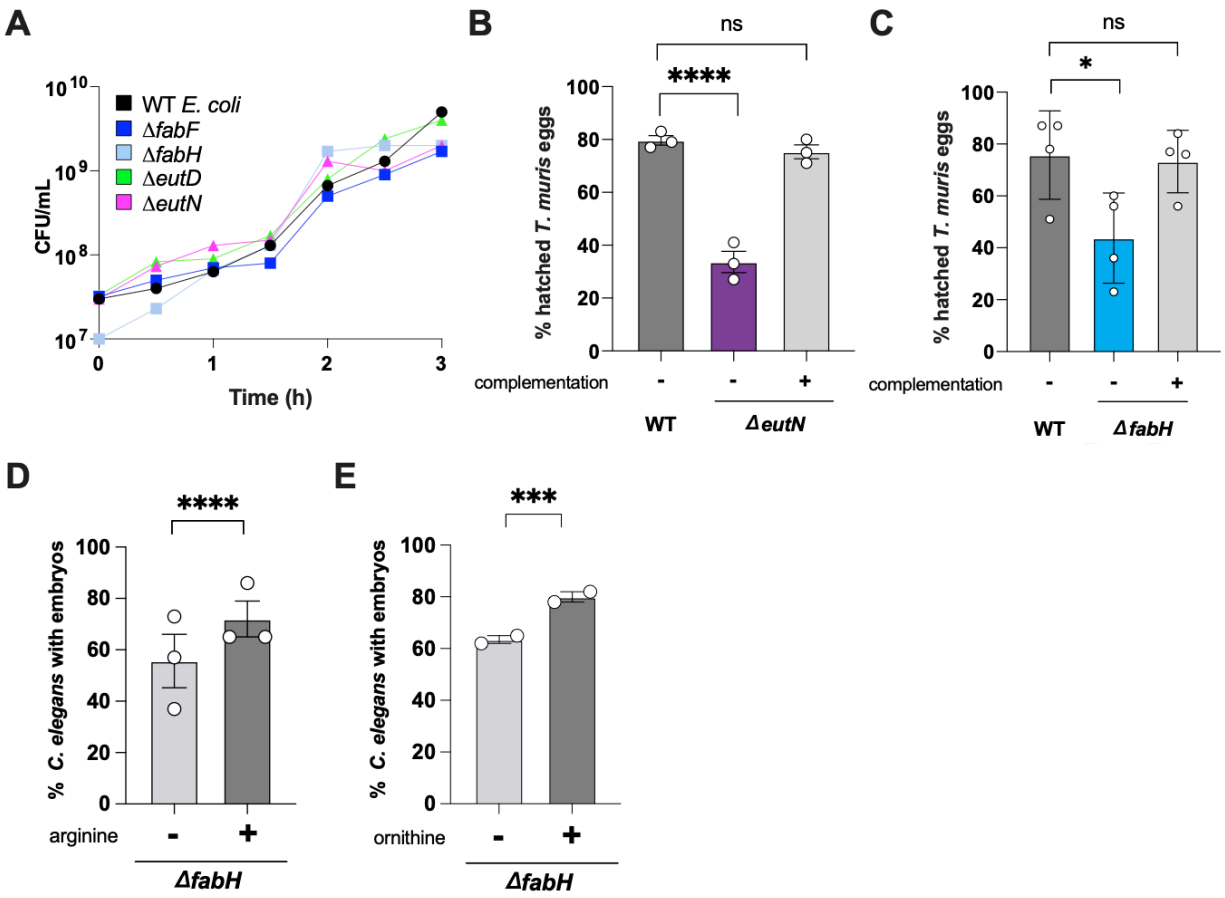

Fig. S2 *E. coli* mutants used for *T. muris* egg hatching assay and effect of arginine and ornithine supplementation on *C. elegans* fertility, related to Fig. 2. **(A)** Bacterial density of monoclonal cultures of each of the strains indicated measured by dilution plating; CFU = colony forming units, h = hours. **(B-C)** Hatching elicited by WT *E. coli* (WT), mutants (B) Δ*eutN* and (C) Δ*fabH***,** and strains where deletions were complemented with a plasmid-borne gene (n = 3-4). One-way analysis of variance (ANOVA) with Dunnett's post-test compared with WT. **(D-E)** Percentage of *C. elegans* Day 1 adults with embryos raised on Δ*fabH E. coli* with arginine or ornithine supplementation. Fisher's exact test (Δ*fabH* alone plus or minus supplementation with 500μM arginine or 100μM ornithine); Total n number of worms scored (left to right): (D) 237, 300 and (E) 216, 149. For all panels, measurements were taken from distinct samples. Data represent the average of at least two independent experiments. Graphs show means and SEM. * $p < 0.05$, *** $p < 0.001$, **** $p < 0.0001$. ns = not significant.

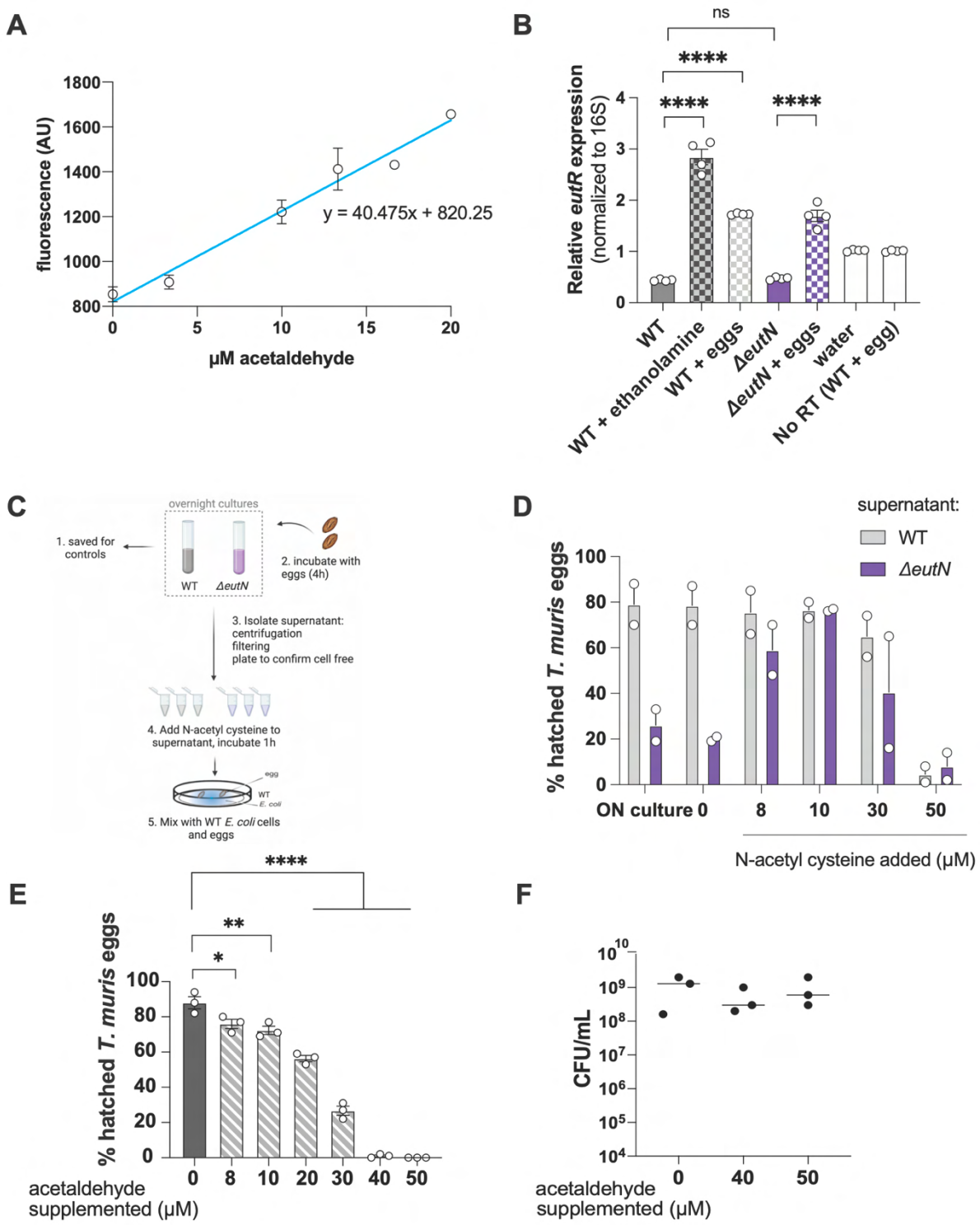

Fig. S3 *E. coli*-derived and exogenous aldehydes reduce *T. muris* egg hatching, related to Fig. 3. (A) DarkZone standard curve for acetaldehyde. Fluorescence

intensity of samples incubated with known concentrations of acetaldehyde and 20μM DarkZone dye (n = 2). AU, arbitrary units. **(B)** Relative *eutR* expression in *E. coli* cells. eggs = pre-incubation with *T. muris* eggs for 4 hours. No RT = no reverse transcriptase control. Data pooled from 2 independent experiments. Analyzed using ANOVA with Tukey's multiple comparisons test. **(C)** Diagram of N-acetyl cysteine supplementation assay. Created using BioRender.com. **(D)** Quantification of hatching rates for mixtures containing WT *E. coli* cells and filtered supernatants supplemented with N-acetyl cysteine at the concentrations indicated (n = 2). **(E)** Quantification of hatching rates for *T. muris* eggs incubated with WT *E. coli* cultures supplemented with acetaldehyde at concentrations indicated (n = 3). Analyzed using ANOVA with Dunnett's post-test compared to 0. **(F)** Bacterial density of conditions indicated from (E) measured by dilution plating (n = 3). For all panels, measurements were taken from distinct samples. Graphs show means and SEM. * $p < 0.05$, ** $p < 0.01$, **** $p < 0.0001$.

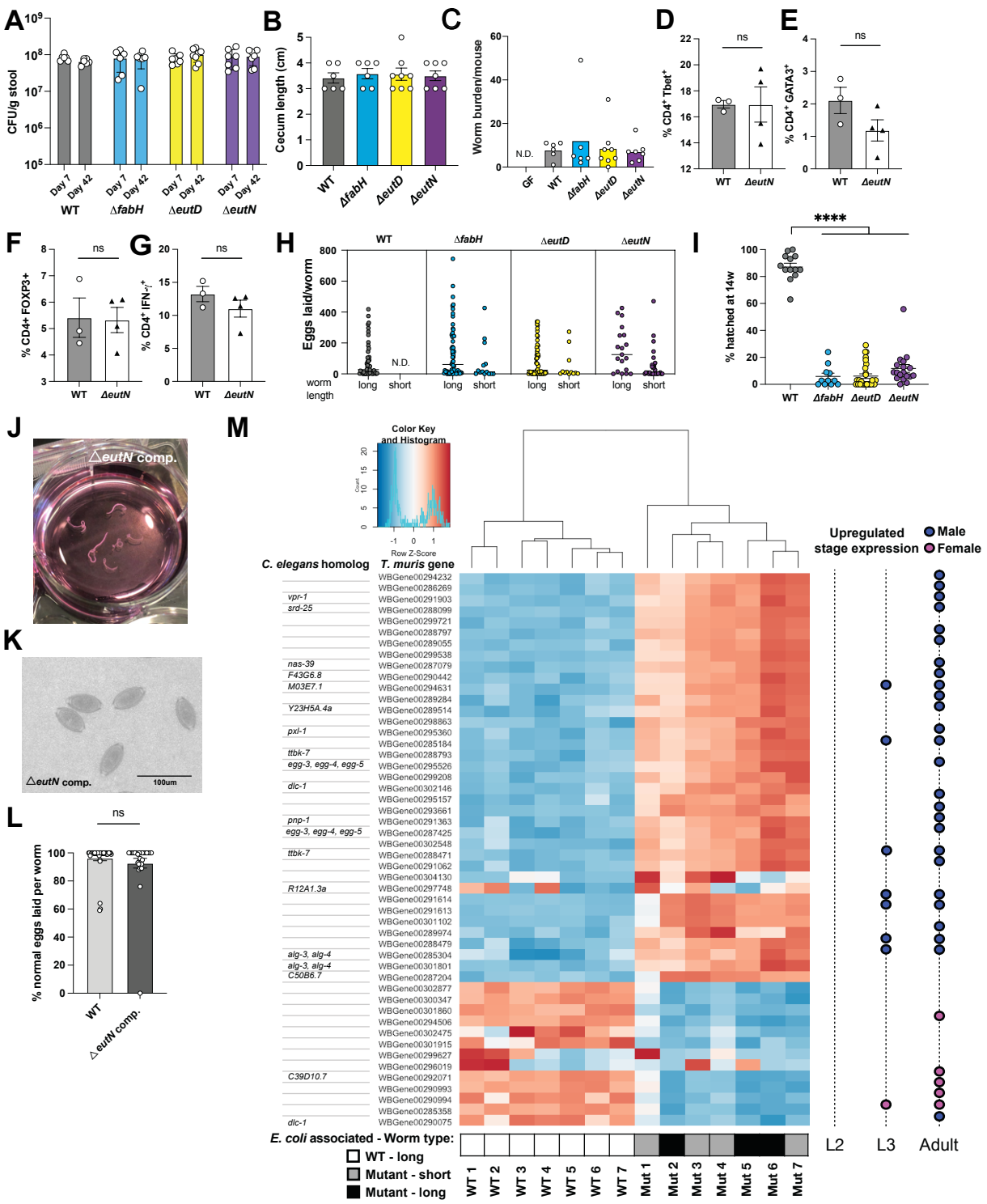

Fig. S4 *T. muris* infection of germ-free and monocolonized mice, related to Fig 4.

(A) *E. coli* burden 7 dpi and 42 dpi (day of sacrifice) in stool of mice gavaged with 1x

10^8 CFU of strains indicated (n = 6-9 mice per group). **(B)** Cecum measurements taken on day of sacrifice for mice in (A). **(C)** Total worms harvested per mouse for germ-free (GF) and mice monocolonized with *E. coli* strains indicated; N.D. = not detected. **(D-G)** $CD4^+$ T cell percentage from mesenteric lymph nodes of WT and *ΔeutN* monocolonized mice. (D) Th1 ($Tbet^+$), (E) Th2 ($GATA3^+$), (F) Treg ($FOXP3^+$). (G) Cells were also stimulated with PMA and ionomycin and stained for intracellular IFN-γ expression, a cytokine known to be positively correlated with host susceptibility to *T. muris*. **(H)** Quantification of eggs laid per worm disaggregated by worm length. Short worms measured < 1 cm. N.D. = not detected. Harvested worms were incubated in individual wells of a 48-well plate with RPMI medium overnight and eggs laid were quantified using light microscopy. **(I)** Percentage of eggs subjected to 14 weeks of embryonation that hatched after incubation with WT *E. coli*. **(J)** Representative image of worms harvested from mice monocolonized with *ΔeutN* strain where *eutN* has been complemented on a plasmid = *ΔeutN* comp. (WT, n = 9; *ΔeutN* comp., n = 8). **(K)** Representative image of eggs laid by worms harvested from mice monocolonized with *ΔeutN* comp. **(L)** Proportion of total eggs laid per worm with normal morphology. Circles represent individual worms (WT, n = 36; *ΔeutN* comp., n = 29). **(M)** Heatmap of the 50 most differentially detected genes between WT- and mutant-associated worms generated using DESeq2. Colors indicate Row Z-score and clusters of genes with similar trends in expression between samples. Red indicates upregulated genes and blue indicates downregulated genes. WT = wildtype *E. coli*. L = *T. muris* larval stage. For all panels, measurements were taken from distinct samples. Data pooled from two independent experiments. Graph shows means and SEM. **** $p < 0.0001$.

Table S1 Top candidates and bacterial gene function (EcoCyc). *Fab* and *eut* genes were chosen for further characterization.

GENE	PROTEIN FUNCTION	FUNCTIONAL GROUP
fabF	β-ketoacyl-[acyl carrier protein] synthase II	Fatty acid biosynthesis
fabH	β-ketoacyl-[acyl carrier protein] synthase III	Fatty acid biosynthesis
eutD	phosphate acetyltransferase	Ethanolamine utilization
eutN	putative ethanolamine catabolic microcompartment shell protein	Ethanolamine utilization
pta	phosphate acetyltransferase	Ethanolamine utilization
rfaF	ADP-heptose—LPS heptosyltransferase 2	Lipopolysaccharide biosynthesis
rfaH	transcription antiterminator RfaH	Lipopolysaccharide biosynthesis
cmoA	carboxy-*S*-adenosyl-L-methionine synthase	Uridine modification in RNA
yhgN	putative inner membrane protein	Antibiotic resistance
holD	DNA polymerase III subunit ψ	DNA replication

Table S2 Single-worm Seq sample metadata, related to Figures 4 and S4. Data for *T. muris* worms subjected to RNA extraction and sequencing analysis.

Worm ID	Sample name	run	*E. coli* associated	Worm length	Eggs laid	% normal eggs laid overnight
WT 1	**MV4**	1	wildtype	long	575	96
WT 2	**MV5**	1	wildtype	long	122	100
WT 3	**MV17**	2	wildtype	long	17	100
WT 4	**MV18**	2	wildtype	long	66	100
WT 5	**MV19**	2	wildtype	long	46	100
WT 6	**MV1**	1	wildtype	long	10	100
WT 7	**MV3**	1	wildtype	long	759	96
Mut 1	**MV24**	2	⊿eutN	short	59	2
Mut 2	**MV40**	2	⊿eutD	long	1	0
Mut 3	**MV30**	2	⊿eutD	short	2	0
Mut 4	**MV33**	2	⊿eutD	short	14	7
Mut 5	**MV35**	2	⊿eutD	long	1	0
Mut 6	**MV14**	1	⊿eutN	long	2	0
Mut 7	**MV32**	2	⊿eutD	short	6	0

Table S3 List of top 50 differentially detected genes, related to Figure S4E. Information was collated from WormBase (version WS283) and Foth et al. (2014) for stage specific expression data. *C. elegans* homologs were found using WormBase BLAST/BLAT.

T. muris gene WormBase ID (primary identifier)	WormBase Annotation	Gene Name	Other name	Seq Length (AA)	Stage specific exp (L2 vs L3, L3 vs. adult, male vs. female) (Foth et al. 2014)	*C. elegans* blast/alignment	Evalue if < 1			*C. elegans* gene(s) brief descriptions from WormBase WormMine		
Increased expression in mutant-assoc. worms												
WBGene00294232	Is predicted to enable calcium ion binding activity.	TMUE_2000009514	TMUE_s0173000900	501	up in adults, male							
WBGene00286269	n/a, protein coding	TMUE_2000006815	TMUE_s0008011000	441	up in adults, male							
WBGene00291903	Is predicted to encode a protein with the following domains: MSP (Major sperm protein) domain; Major sperm protein (MSP) domain; PapD-like superfamily; Immunoglobulin-like fold; and Vesicle-associated membrane-protein-associated protein.	TMUE_2000006496	TMUE_s0088003400	168	up in adults, male	30% ID, 48% +	2.00E-08	vpr-1	WBGene00018008	vpr-1 encodes the C. elegans VAP (VAMP-associated protein) ortholog, a transmembrane protein containing an N-terminal extracellular major sperm protein (MSP) domain; loss of vpr-1 function during development indicates that vpr-1 is required, both in vab-1-dependent and vab-1-independent pathways, for proper distal tip cell migration during somatic gonad development, ventral hypodermal cell migrations during embryonic enclosure, and anteriorly directed amphid neuron migration; like C. elegans MSPs, injection of the VPR-1 MSP domain into fog-2 females induces oocyte maturation and gonadal sheath cell contraction; the VPR-1 MSP domain directly binds the VAB-1/Ephrin receptor extracellular domain in vitro and in vivo, binds the oocyte and gonadal sheath cell plasma membranes.		
WBGene00288099	n/a, protein coding	TMUE_1000004904	TMUE_s0023007200	151	up in adults, male	34% ID, 64% +	0.77	srd-25	WBGene00005103	Serpentine receptor class delta-25		
WBGene00299721	n/a, protein coding	TMUE_2000006814		175								
WBGene00288797	n/a, protein coding	TMUE_1000005514	TMUE_s0032005600	539	up in adults, male							
WBGene00289055	Is predicted to encode a protein with the following domain: Rho GTPase activation protein.	TMUE_2000010584	TMUE_s0036003300	454	up in adults, male							
WBGene00299538	n/a, protein coding	TMUE_2000006270		113								
WBGene00287079	n/a, protein coding	TMUE_3000013015	TMUE_s0014002100	421	up in adults, male	27% ID, 45% +	0.37	nas-39	WBGene00003555	Zinc metalloproteinase nas-39	nas-39 encodes an astacin family zinc metalloprotease and the only BMP-1/Tolloid homolog in C. elegans; in Drosophila and vertebrates nas-39 homologues activate TGF-beta signals by cleaving chordin/SOG, an inhibitor keeping the TGF-beta in inactive form; however developmental processes known to be affected by TGF-beta signaling are unaffected in nas-39 mutants, suggesting that nas-39 is not required for TGF-beta signaling; nas-39 is expressed in the pharynx, intestine, vulval and body wall muscles, and many neurons.	
WBGene00290442	n/a, protein coding	TMUE_1000005106	TMUE_s0058002100	237	up in adults, male	26% ID, 52% +	0.19	F43G6.8	WBGene00009660	RING-type domain-containing protein		
WBGene00294631	Is predicted to encode a protein with the following domains: MSP (Major sperm protein) domain; Major sperm protein (MSP) domain; PapD-like superfamily; and Immunoglobulin-like fold.	TMUE_1000003930	TMUE_s0204000100	239	up in L3, adult, male	47% ID, 75% +		M03E7.1	WBGene00019753	major sperm protein		
WBGene00289284	n/a, protein coding	TMUE_2000007553	TMUE_s0039002800	183	up in adults, male							
WBGene00289514	Is predicted to encode a protein with the following domains: MSP (Major sperm protein) domain; Major sperm protein (MSP) domain; PapD-like superfamily; and Immunoglobulin-like fold.	TMUE_3000012031	TMUE_s0042005600	217	up in adults, male	29% ID, 52% +	4.00E-06	Y23H5A.4a	WBGene00021271	major sperm protein		
WBGene00298863	Is predicted to encode a protein with the following domains: Zinc finger, C2H2 type; Zinc finger C2H2-type; and Zinc finger C2H2 superfamily.	TMUE_1000004114		539								
WBGene00295360	Is predicted to encode a protein with the following domains: LIM domain and Zinc finger, LIM-type.	TMUE_1000004317	TMUE_s0284000100	139	up in adults, male	29% ID, 48% +	1.00E-13	pxl-1	WBGene00016197	pxl-1 encodes proteins containing N-terminal LD motifs and C-terminal LIM domains that is the C. elegans ortholog of vertebrate paxillin; pxl-1 is required for organized myofilament structure in the pharynx and pharyngeal muscle contraction, and hence feeding and viability past the first larval stage; PXL-1 is expressed in body wall and pharyngeal muscle, as well as pharyngeal epithelial cells; PXL-1 localizes to sites of actin attachment, namely dense bodies, adhesion plaques, and M-lines in body wall muscle, and podosome-like structures in pharyngeal muscle; pxl-1 expression in pharyngeal muscle and marginal cells is sufficient to rescue the pharyngeal muscle defects and lethality of a pxl-1 mutant; PXL-1 physically interacts with muscle proteins DEB-1, UIG-1, LIM-8, UNC-96, UNC-95, and HUM-6.		
WBGene00285184	n/a, protein coding	TMUE_1000003466	TMUE_s0002000500	528	up in L3, adults, male							
WBGene00288793	Is predicted to enable ATP binding activity and protein kinase activity.	TMUE_1000003767		339		38% ID, 62% +	3.00E-51	ttbk-7	WBGene00011283	Protein kinase domain-containing protein		
WBGene00295526	Is predicted to enable protein tyrosine phosphatase activity. Is an ortholog of C. elegans egg-5; egg-3; and egg-4.	TMUE_3000014972	TMUE_s0323000100	366	up in adults, male			egg-3, egg-4, egg-5	WBGene00009701, WBGene00020652, WBGene00020035	egg-3 encodes a member of the protein tyrosine phosphatase-like (PTPL) family; EGG-3 activity is required for proper regulation of the cell surface and cortical rearrangements that occur during egg activation in response to sperm entry; EGG-3 physically interacts with EGG-4/5 and the MBK-2 kinase to sequester MBK-2 at the oocyte cortex prior to meiosis, thus preventing MBK-2 from phosphorylating its substrates, such as cytoplasmic MEI-1/katanin; EGG-3 initially localizes to the oocyte cortex, but during anaphase of meiosis I moves into the cytoplasm where it is degraded allowing for activation of MBK-2.	egg-4 encodes a pseudotyrosine phosphatase; egg-4, along with egg-5 which also encodes a pseudotyrosine phosphatase, are required for the egg-to-oocyte transition and embryonic development; EGG-4 and EGG-5 function to negatively regulate the activity of the MBK-2 DYRK family kinase by sequestering MBK-2 at the oocyte cortex and, in the case of EGG-4, by inhibiting its enzymatic activity; EGG-4 physically interacts with MBK-2 and in in vitro assays, appears to function as a mixed-type inhibitor of MBK-2 kinase activity; EGG-4 localizes to the oocyte cortex and nuclei.	egg-5 encodes a pseudotyrosine phosphatase; egg-5, along with egg-4 which also encodes a pseudotyrosine phosphatase, are required for the egg-to-oocyte transition and embryonic development; EGG-4 and EGG-5 function to negatively regulate the activity of the MBK-2 DYRK family kinase by sequestering MBK-2 at the oocyte cortex and, in the case of EGG-4, by inhibiting its enzymatic activity; EGG-5 physically interacts with MBK-2; EGG-5 localizes to the oocyte cortex and nuclei.
WBGene00299208		TMUE_1000005104		96								
WBGene00302146	Is predicted to encode a protein with the following domains: Dynein light chain type 1; Dynein light chain, type 1/2; and Dynein light chain superfamily.	TMUE_3000014161		92		41% ID, 64% +	4.00E-16	dlc-1	WBGene00001005	dlc-1 encodes a dynein light chain 1, required for viability, that inhibits DHC-1 in vivo; DLC-1 is 92-95% identical to its orthologs human DYNLL1 (OMIM:601562) and DYNLL2 (OMIM:608942); DLC-1 is paralogous to DLC-2/-6; DLC-1 is expressed in adult body wall muscle, and in larval and adult pharynx, posterior intestine, and nervous system (e.g., ventral nerve cord, head neurons, and tail neurons); dlc-1 is probably transcriptionally activated by DAF-19; DLC-1 is required for normal embryonic and larval viability, embryonic pronuclear migration, growth speed, fertility, brood size, body shape, and cuticular integrity; anterograde movements of DLC-1 in neurons are regulated by PTL-1/Tau.		
WBGene00295157	n/a, protein coding	TMUE_3000012749	TMUE_s0255000300	221	up in adults, male							
WBGene00293661	n/a, protein coding	TMUE_2000008700	TMUE_s0144002900	72	up in adults, male							
WBGene00291363	Is predicted to enable purine-nucleoside phosphorylase activity. Is an ortholog of C. elegans K02D7.1. In C. elegans, K02D7.1 is involved in innate immune response.	TMUE_1000004881	TMUE_s0076001400	275	up in adults, male	32% ID, 55% +	5.00E-33	pnp-1		K02D7.1 is orthologous to the human gene PURINE NUCLEOSIDE PHOSPHORYLASE (NP; OMIM:164050), which when mutated leads to disease.		
WBGene00287425	Is predicted to enable protein tyrosine phosphatase activity. Is an ortholog of C. elegans egg-5; egg-3; and egg-4.	TMUE_2000006534	TMUE_s0016011300	445	up in adults, male			egg-3, egg-4, egg-5	WBGene00009701, WBGene00020652, WBGene00020035	egg-3 encodes a member of the protein tyrosine phosphatase-like (PTPL) family; EGG-3 activity is required for proper regulation of the cell surface and cortical rearrangements that occur during egg activation in response to sperm entry; EGG-3 physically interacts with EGG-4/5 and the MBK-2 kinase to sequester MBK-2 at the oocyte cortex prior to meiosis, thus preventing MBK-2 from phosphorylating its substrates, such as cytoplasmic MEI-1/katanin; EGG-3 initially localizes to the oocyte cortex, but during anaphase of meiosis I moves into the cytoplasm where it is degraded allowing for activation of MBK-2.	egg-4 encodes a pseudotyrosine phosphatase; egg-4, along with egg-5 which also encodes a pseudotyrosine phosphatase, are required for the egg-to-oocyte transition and embryonic development; EGG-4 and EGG-5 function to negatively regulate the activity of the MBK-2 DYRK family kinase by sequestering MBK-2 at the oocyte cortex and, in the case of EGG-4, by inhibiting its enzymatic activity; EGG-4 physically interacts with MBK-2 and in in vitro assays, appears to function as a mixed-type inhibitor of MBK-2 kinase activity; EGG-4 localizes to the oocyte cortex and nuclei.	egg-5 encodes a pseudotyrosine phosphatase; egg-5, along with egg-4 which also encodes a pseudotyrosine phosphatase, are required for the egg-to-oocyte transition and embryonic development; EGG-4 and EGG-5 function to negatively regulate the activity of the MBK-2 DYRK family kinase by sequestering MBK-2 at the oocyte cortex and, in the case of EGG-4, by inhibiting its enzymatic activity; EGG-5 physically interacts with MBK-2; EGG-5 localizes to the oocyte cortex and nuclei.
WBGene00302548	Is predicted to encode a protein with the following domains: Histidine phosphatase superfamily (branch 1); Histidine phosphatase superfamily, clade-1; and Histidine phosphatase superfamily.	TMUE_1000004837	TMUE_0105002600	229								

WBGene00288471	Is predicted to enable ATP binding activity and protein kinase activity. Is an ortholog of C. elegans M7.7.	TMUE_3000014681	TMUE_s002803500	361	up in L3, adults, male	28% ID, 49% +	4.00E-38	ttbk-7	WBGene00011283	Protein kinase domain-containing protein		
WBGene00291062	n/a, protein coding	TMUE_1000005581	TMUE_s007001900	163	up in adults, male							
WBGene00304130	n/a, n/a	TMUE_0100000692		n/a								
WBGene00297748	Is predicted to enable peptidase inhibitor activity.	TMUE_0000001881		94		41% ID, 52% +	0.87	R12A1.3a	WBGene00020017	BPTI/Kunitz inhibitor domain-containing protein		
WBGene00291614	Is predicted to encode a protein with the following domain: Cystine-knot cytokine.	TMUE_3000010896	TMUE_s008203800	286	up in L3, adults, male							
WBGene00291613	Is predicted to encode a protein with the following domain: Cystine-knot cytokine.	TMUE_3000010897	TMUE_s008203700	297	up in L3, adults, male							
WBGene00301102	n/a, protein coding	TMUE_3000010898		286								
WBGene00289974	n/a, protein coding	TMUE_3000013584	TMUE_s005005900	84	up in adults, male							
WBGene00288479	Is predicted to enable nucleic acid binding activity. Is an ortholog of C. elegans alg-3 and alg-4. In C. elegans, alg-4 Is involved in spermatogenesis.	TMUE_3000012542	TMUE_s002804300	918	up in L3, adults, male			alg-3, alg-4	WBGene00011910, WBGene00006449	alg-3 encodes an Argonaute (AGO) protein that is a member of the AGO clade of Argonaute small RNA-binding proteins; together with its paralog, alg-4, alg-3 is required for normal brood sizes at elevated temperatures, specifically for the process of spermiogenesis in which spermatids are converted to mobile ameboid sperm; alg-3/4 is also required for accumulation of male germline-specific 26G-RNAs, suggesting that alg-3/4 mediate thermotolerant fertility via a 26G-RNA-mediated pathway; a GFP::ALG-3 rescuingfusion protein is expressed in germ cells during spermatogenesis and localizes to the cytoplasm and to P granules.	alg-4: encodes an Argonaute (AGO) protein that is a member of the AGO clade of Argonaute small RNA-binding proteins; together with its paralog, alg-3, alg-4 is required for normal brood sizes at elevated temperatures, specifically for the process of spermiogenesis in which spermatids are converted to mobile ameboid sperm; alg-3/4 is also required for accumulation of male germline-specific 26G-RNAs, suggesting that alg-3/4 mediate thermotolerant fertility via a 26G-RNA-mediated pathway.	
WBGene00285304	Is predicted to enable nucleic acid binding activity. Is an ortholog of C. elegans alg-3 and alg-4. In C. elegans, alg-4 Is involved in spermatogenesis.	TMUE_1000003405	TMUE_s000203100	880	up in L3, adults, male			alg-3, alg-4	WBGene00011910, WBGene00006449	alg-3 encodes an Argonaute (AGO) protein that is a member of the AGO clade of Argonaute small RNA-binding proteins; together with its paralog, alg-4, alg-3 is required for normal brood sizes at elevated temperatures, specifically for the process of spermiogenesis in which spermatids are converted to mobile ameboid sperm; alg-3/4 is also required for accumulation of male germline-specific 26G-RNAs, suggesting that alg-3/4 mediate thermotolerant fertility via a 26G-RNA-mediated pathway; a GFP::ALG-3 rescuingfusion protein is expressed in germ cells during spermatogenesis and localizes to the cytoplasm and to P granules.	alg-4: encodes an Argonaute (AGO) protein that is a member of the AGO clade of Argonaute small RNA-binding proteins; together with its paralog, alg-3, alg-4 is required for normal brood sizes at elevated temperatures, specifically for the process of spermiogenesis in which spermatids are converted to mobile ameboid sperm; alg-3/4 is also required for accumulation of male germline-specific 26G-RNAs, suggesting that alg-3/4 mediate thermotolerant fertility via a 26G-RNA-mediated pathway.	
WBGene00301801	n/a, protein coding	TMUE_3000013156		145								
WBGene00287204	Is predicted to enable alpha-amylase activity and cation binding activity. Is an ortholog of C. elegans C50B6.7.	TMUE_2000009275	TMUE_2000009275	695				C50B6.7	WBGene00008220	predicted to enable alpha-amylase activity; alpha-amylase activity (releasing maltohexaose); and metal ion binding activity. Is expressed in intestine. Is an ortholog of human AMY2A (amylase alpha 2A) and AMY2B (amylase alpha 2B).		
Decreased expression in mutant-assoc worms												
WBGene00302877	n/a, protein coding	TMUE_3000012979	TMUE_0010004200	313								
WBGene00300347	n/a, protein coding	TMUE_2000008654		142								
WBGene00301860	n/a, protein coding	TMUE_3000013344		781								
WBGene00294506	Is predicted to encode a protein with the following domains: TspO/MBR family; TspO/MBR-related protein; and TspO/MBR-related superfamily.	TMUE_1000004599	TMUE_s019400800	238	up in adults, female							
WBGene00302475	n/a, protein coding	TMUE_1000003336	TMUE_005800 4600	174								
WBGene00301915	n/a, protein coding	TMUE_3000013424		277								
WBGene00299627	n/a, protein coding	TMUE_2000006504		69								
WBGene00296019	Is predicted to encode a protein with the following domain: .	TMUE_0000000071		136								
WBGene00292071	Is predicted to enable chitin binding activity. Is an ortholog of C. elegans C39D10.7.	TMUE_3000014378	TMUE_s009205000	842	up in adults, female	23% ID, 34% +	8.00E-20	C39D10.7	WBGene00016534	C39D10.7 encodes a large (1185-residue) protein with 11 chitin-bindingperitrophin-A domains; C39D10.7 transcripts are enriched inhermaphrodites; like CEJ-1 and CPG-2, C39D10.7 might participate ineggshell synthesis and early embryonic development, and C39D10.7'smultiple peritrophin-A domains might enable mechanical cross-linking ofchitin; however, C39D10.7 alone has no visible function in mass RNAiassays.		
WBGene00290993	n/a, protein coding	TMUE_3000014020	TMUE_s006902000	166	up in adults, female							
WBGene00290994	n/a, protein coding	TMUE_3000011882	TMUE_s006902100	947	up in adults, female							
WBGene00285358	Is predicted to enable lipid binding activity.	TMUE_1000003367	TMUE_s000203100	2006	up in L3, adults, female							
WBGene00290975	n/a, protein coding	TMUE_3000011875	TMUE_s006900200	90	up in adults, male	33% ID, 51% +	4.00E-16	dlc-1	WBGene00001005	dlc-1 encodes a dynein light chain 1, required for viability, that inhibits DHC-1 in vivo; DLC-1 is 92-95% identical to its orthologs human DYNLL1 (OMIM:601562) and DYNLL2 (OMIM:608942); DLC-1 is paralogous to DLC-2/-6; DLC-1 is expressed in adult body wall muscle, and in larval and adult pharynx, posterior intestine, and nervous system (e.g., ventral nerve cord, head neurons, and tail neurons); dlc-1 is probably transcriptionally activated by DAF-19; DLC-1 is required for normal embryonic and larval viability, embryonic pronuclear migration, growth speed, fertility, brood size, body shape, and cuticular integrity; anterograde movements of DLC-1 in neurons are regulated by PTL-1/Tau.		

Table S4 Strains used in this study.

STRAIN	SPECIES	GENOTYPE	REFERENCE
BW25113	*E. coli*	*F-, Δ(araD-araB)567, ΔlacZ4787*(::rrnB-3), *λ-, rph-1, Δ(rhaD-rhaB)568, hsdR514*	(Baba et al., 2006)
GC833	*C. elegans*	*glp-1(ar202)* III	(Pepper et al., 2003)
GC1250	*C. elegans*	*daf-16(m26) I*; *daf-2(e1370) glp-1(e2141)* III	(Michaelson et al., 2010)
GC1474	*C. elegans*	*glp-1(e2141)* III; *hjSi20* [*Pmyo-2P::mCherry::unc-54* 3'UTR] IV; *zuIs70* [pJN152: *end-1P::gfp::caax; unc-119*(+)] V	This study
GC1545	*C. elegans*	*daf-5(e1386) II; glp-1(e2141)* III	This study
GC1547	*E. coli*	BW25113 transformed with pET28	This study
GC1549	*E. coli*	BW25113 Δf*abF*::*kan*	This study
GC1558	*E. coli*	BW25113 Δ*eutN*::kan, pGC735	This study
GC1559	*E. coli*	BW25113 Δf*abH*::kan, pGC738	This study
GC1643	*E. coli*	BW25113 Δ*eutC::kan*	This study
GC1644	*E. coli*	BW25113 Δ*eutC*	This study
GC1645	*E. coli*	BW25113 Δ*eutN::kan*	This study
GC1646	*E. coli*	BW25113 Δ*eutN*	This study
GC1647	*E. coli*	BW25113 Δ*eutC* Δ*eutN::kan*	This study
GC1648	*E. coli*	BW25113 Δ*eutC::kan* Δ*eutN*	This study
GC1649	*E. coli*	BW25113 Δ*eutD*	This study
GC1650	*E. coli*	BW25113 Δ*eutD* pPlac-eutD	This study
JW1077	*E. coli*	BW25113 Δ*fabH::kan*	(Baba et al., 2006)
JW2442	*E. coli*	BW25113 Δ*eutD*::kan	
JW2440	*E. coli*	BW25113 Δ*eutN*::*kan*	

JW2294	*E. coli*	BW25113 Δ*pta*::*kan*	
JW3595	*E. coli*	BW25113 Δ*rfaF*::*kan*	
JW3818	*E. coli*	BW25113 *ΔrfaH*::*kan*	
JW4334	*E. coli*	BW25113 Δ*holD*::*kan*	
JW1859	*E. coli*	BW25113 Δ*cmoA*::*kan*	
JW3397	*E. coli*	BW25113 Δ*yhgN*::*kan*	
JW3929	*E. coli*	BW25113 Δ*argE::kan*	
JW3932	*E. coli*	BW25113 Δar*gH*::*kan*	

Table S5 Primers used in this study.

Primer	Details
GCo2700 – 5'…. CCGCGCTGGTTCGTTTCtagTGCAGCAATGGCAACAACGTTG	Forward primer- vector fragment to amplify pBR322 for Gibson assembly with PCR product bearing wild-type *fabH* sequence
GCo2701 – 5'…. ACGTTGTTGCCATTGCTGCActaGAAACGAACCAGCGCG	Reverse primer- vector fragment to amplify pBR322 for Gibson assembly with PCR product bearing wild-type *fabH* sequence
GCo2702 – 5'…. AGCTGTCAAACATGAGAATTATAACCGAAAAGTGACTGAGCGTACa	Forward primer- *fabH* coding sequence for Gibson assembly with pBR322
GCo2703 – 5'…. CTCAGTCACTTTTCGGTTATAATTCTCATGTTTGACAGCTTATCATCGATAAG	Reverse primer- *fabH* coding sequence for Gibson assembly with pBR322
GCo2708 – 5'…. agctgtcaaacatgagaattAATACGCCACGGAGGCG	Forward primer- *eutN* coding sequence for Gibson assembly with pBR322
GCo2709 – 5'…. acgttgttgccattgctgcattaTTTGTGGAAAATTACCTGACCGCC	Reverse primer- *eutN* coding sequence for Gibson assembly with pBR322
GCo2710 – 5'…. ACCCGCCTCCGTGGCGTATTaattctcatgtttgacagcttatcatcgataag	Forward primer- vector fragment to amplify pBR322 for Gibson assembly with PCR product bearing wild-type *eutN* sequence
GCo2711 – 5'…. AGGTAATTTTCCACAAAtaatgcagcaatggcaacaacgt	Reverse primer- vector fragment to amplify pBR322 for Gibson assembly

	with PCR product bearing wild-type *eutN* sequence
GCo2744 – 5'…. GCCGGGAAGCTAGAGTAAGTAGT	pBR322 forward (used to confirm gene sequence)
GCo2745 – 5'…. AAAAACATATGATTATTGAACGTTGTCGTG	Forward primer- *eutD* coding sequence with an NdeI site for cloning into pPlacRppH6
GCo2746 – 5'…. TTTTTTTCTAGAGTTCATTCAACCAGTGTTTGTAAAC	Reverse primer- *eutD* coding sequence with an XbaI site for cloning into pPlacRppH6
GCo2747 – 5'…. CGCGTTGGCCGATTCATTAATGCAGC	pPlacRppH6 forward (used to confirm gene sequence)
GCo2748 – 5'…. GCTTCGCAACGTTCAAATCCGCTCC	pPlacRppH6 reverse (used to confirm gene sequence)
ACTCCTACGGGAGGCAGCAGT	Forward primer- 16S coding sequence for qPCR
ATTACCGCGGCTGCTGGC	Reverse primer- 16S coding sequence for qPCR
GGGAGGCACCGAGTTTGAA	Forward primer- *eutR* coding sequence for qPCR
GGGAGGCACCGA GTTTGAA	Reverse primer- *eutR* coding sequence for qPCR

Table S6 Plasmid names and descriptions.

Plasmid name	**Description**
pGC735	*eutN* cloned into pBR322 by Gibson assembly
pGC737	pET28
pGC738	*fabH* cloned into pBR322 by Gibson assembly

pPlac-eutD	*eutD* under the control of a *lac*UV5 promoter
pBR322	pBR322

Table S7 Primer sequences to verify kan cassette insertion within target genes.

GCo296 AGCTTTGAAGTATTACGCCCGGAC	**Forward PCR primer *eutD***
GCo2797 CCTTTCGAGCACGGTCTACG	**Forward sequencing primer *eutD***
GCo2798 AACACCAACCAGCTTGACGC	**Reverse PCR primer *eutD***
GCo2799 AGGCCCCGGGTTTCGATC	**Reverse sequencing primer *eutD***
GCo2800 CTTCCCGATCGGCCTGAAAGG	**Forward PCR primer *eutN***
GCo2801 CTGTAATCACCCTGTGTGACGTCG	**Forward sequencing primer *eutN***
GCo2802 ACTTTGGCTGCCGCAACGGC	**Reverse PCR primer *eutN***
GCo2803 CGCGAAAACGCCCATCTCATG	**Reverse sequencing primer *eutN***
GCo2804 AATTGCCGCTCGCCTGGA	**Forward PCR primer *fabH***

GCo2805 GGTTTTGAGCTGCTGGACGG	**Forward sequencing primer *fabH***
GCo2806 GCCGCAGAAGCTTCAGCAAAC	**Reverse PCR primer *fabH***
GCo2807 GGATAGCTCGCCGCCATATCA	**Reverse sequencing primer *fabH***
GCo2808 GTCCTGCGGTGGTTATCCCAA	**Forward PCR primer *pta***
GCo2809 AAGAACTGGTTATCGCGCAAG	**Forward sequencing primer *pta***
GCo2810 AAGTGGGATGGCGCAATTCAT	**Reverse PCR primer *pta***
GCo2811 GCAGCGCAGTTAAGCAAGATAA	**Reverse sequencing primer *pta***
GCo2812 AATCACCACCGTTCAGGCTGC	**Forward PCR primer *fabF***
GCo2813 GCCACCAGGCGTAAGTGAAC	**Forward sequencing primer *fabF***
GCo2814 CCGTTAATTAAGAACATACCGGCTCC	**Reverse PCR primer *fabF***

GCo2815 AGTGTGGCAGCATGTTCACTACG	**Reverse sequencing primer *fabF***
GCo2832 AACTGAAAGGCCGCTATCAGG	**Forward PCR primer** ***rfaF***
GCo2833 GGTTACGACAAACCGTTCAAAACC	**Forward sequencing primer *rfaF***
GCo2834 GCCAGGAAGGAATCTGTGCGAA	**Reverse PCR primer** ***rfaF***
GCo2835 CCACCCAGTCAAACTTAATCCCTG	**Reverse sequencing primer** ***rfaF***
GCo2836 GGCGTTCATCTTTGCGATGCTG	**Forward PCR primer** ***rfaH***
GCo2837 CTGACGGTATAACGCAAACCGG	**Forward sequencing primer** ***rfaH***
GCo2838 TCTCACGCCAAAGCCATCATCC	**Reverse PCR primer** ***rfaH***
GCo2839 CCATATTTTGCAACGTATTGCGCAC	**Reverse sequencing primer** ***rfaH***
GCo2840 CTCTTGGCACATCTTTCACCATACA	**Forward PCR primer** ***yhgN***
GCo2841	**Forward sequencing primer *yhgN***

CGAAGCCATCAGTAATGCGACTT	
GCo2842 CCGAAACGCTGAAAACCTGGAC	**Reverse PCR primer** ***yhgN***
GCo2843 GGATGATTGCGTTCCAGCTGTT	**Reverse sequencing primer** ***yhgN***
GCo2844 TGTGCGCTGTTGCTGATGGT	**Forward PCR primer** ***cmoA***
GCo2845 TTTGGTATATGCCCTGGGAGTTGG	**Forward sequencing primer** ***cmoA***
GCo2846 GGTAGAAACTCCACCGCATTTGA	**Reverse PCR primer** ***cmoA***
GCo2847 TTAAACAACCCGTGCTGCTGCT	**Reverse sequencing primer** ***cmoA***
GCo2848 TGTGACGCAGCAAGACTTCACT	**Forward PCR primer** ***holD***
GCo2849 ATGCAGACATGGAATGCTCCTCAA	**Forward sequencing primer** ***holD***
GCo2850 ACCACTTGCGTAATCGCAAACG	**Reverse PCR primer** ***holD***
GCo2851 TTGCCGTTTTGCGTTAACTGAAAGT	**Reverse sequencing primer** ***holD***

References

Agarwal, I., Farnow, C., Jiang, J., Kim, K.S., Leet, D.E., Solomon, R.Z., Hale, V.A., and Goutte, C. (2018). HOP-1 Presenilin Deficiency Causes a Late-Onset Notch Signaling Phenotype That Affects Adult Germline Function in Caenorhabditis elegans. Genetics *208*, 745-762.

Antignano, F., Mullaly, S.C., Burrows, K., and Zaph, C. (2011). Trichuris muris infection: a model of type 2 immunity and inflammation in the gut. J Vis Exp.

Baba, T., Ara, T., Hasegawa, M., Takai, Y., Okumura, Y., Baba, M., Datsenko, K.A., Tomita, M., Wanner, B.L., and Mori, H. (2006). Construction of Escherichia coli K-12 in-frame, single-gene knockout mutants: the Keio collection. Mol Syst Biol *2*, 2006 0008.

Bancroft, A.J., Else, K.J., and Grencis, R.K. (1994). Low-level infection with Trichuris muris significantly affects the polarization of the CD4 response. European journal of immunology *24*, 3113-3118.

Boeck, M.E., Huynh, C., Gevirtzman, L., Thompson, O.A., Wang, G., Kasper, D.M., Reinke, V., Hillier, L.W., and Waterston, R.H. (2016). The time-resolved transcriptome of C. elegans. Genome research *26*, 1441-1450.

Bolger, A.M., Lohse, M., and Usadel, B. (2014). Trimmomatic: a flexible trimmer for Illumina sequence data. Bioinformatics *30*, 2114-2120.

Chen, W.W., Freinkman, E., Wang, T., Birsoy, K., and Sabatini, D.M. (2016). Absolute Quantification of Matrix Metabolites Reveals the Dynamics of Mitochondrial Metabolism. Cell *166*, 1324-1337 e1311.

Cheng, K.C.-C., Klancer, R., Singson, A., and Seydoux, G. (2009). Regulation of MBK-2/DYRK by CDK-1 and the pseudophosphatases EGG-4 and EGG-5 during the oocyte-to-embryo transition. Cell *139*, 560-572.

Cherepanov, P.P., and Wackernagel, W. (1995). Gene disruption in Escherichia coli: TcR and KmR cassettes with the option of Flp-catalyzed excision of the antibiotic-resistance determinant. Gene *158*, 9-14.

Conine, C.C., Batista, P.J., Gu, W., Claycomb, J.M., Chaves, D.A., Shirayama, M., and Mello, C.C. (2010). Argonautes ALG-3 and ALG-4 are required for spermatogenesis-specific 26G-RNAs and thermotolerant sperm in Caenorhabditis elegans. Proceedings of the National Academy of Sciences *107*, 3588-3593.

D'Elia, R., Behnke, J.M., Bradley, J.E., and Else, K.J. (2009). Regulatory T cells: a role in the control of helminth-driven intestinal pathology and worm survival. The journal of immunology *182*, 2340-2348.

Dalfo, D., Michaelson, D., and Hubbard, E.J. (2012). Sensory regulation of the C. elegans germline through TGF-beta-dependent signaling in the niche. Curr Biol *22*, 712-719.
Deana, A., Celesnik, H., and Belasco, J.G. (2008). The bacterial enzyme RppH triggers messenger RNA degradation by 5′ pyrophosphate removal. Nature *451*, 355-358.

Dobin, A., Davis, C.A., Schlesinger, F., Drenkow, J., Zaleski, C., Jha, S., Batut, P., Chaisson, M., and Gingeras, T.R. (2013). STAR: ultrafast universal RNA-seq aligner. Bioinformatics *29*, 15-21.

Donohue, T.M., Jr., Tuma, D.J., and Sorrell, M.F. (1983). Acetaldehyde adducts with proteins: binding of [14C]acetaldehyde to serum albumin. Arch Biochem Biophys *220*, 239-246.

Fahmy, M.A. (1954). An investigation on the life cycle of Trichuris muris. Parasitology *44*, 50-57.

Foth, B.J., Tsai, I.J., Reid, A.J., Bancroft, A.J., Nichol, S., Tracey, A., Holroyd, N., Cotton, J.A., Stanley, E.J., and Zarowiecki, M. (2014). Whipworm genome and dual-species transcriptome analyses provide molecular insights into an intimate host-parasite interaction. Nature genetics *46*, 693-700.

Gracida, X., and Eckmann, C.R. (2013). Fertility and germline stem cell maintenance under different diets requires nhr-114/HNF4 in C. elegans. Curr Biol *23*, 607-613.

Hayes, K.S., Bancroft, A.J., Goldrick, M., Portsmouth, C., Roberts, I.S., and Grencis, R.K. (2010). Exploitation of the intestinal microflora by the parasitic nematode Trichuris muris. Science *328*, 1391-1394.

Holm, J.B., Sorobetea, D., Kiilerich, P., Ramayo-Caldas, Y., Estelle, J., Ma, T., Madsen, L., Kristiansen, K., and Svensson-Frej, M. (2015). Chronic Trichuris muris Infection Decreases Diversity of the Intestinal Microbiota and Concomitantly Increases the Abundance of Lactobacilli. PLoS One *10*, e0125495.

Houlden, A., Hayes, K.S., Bancroft, A.J., Worthington, J.J., Wang, P., Grencis, R.K., and Roberts, I.S. (2015). Chronic Trichuris muris Infection in C57BL/6 Mice Causes Significant Changes in Host Microbiota and Metabolome: Effects Reversed by Pathogen Clearance. PLoS One *10*, e0125945.

Hubbard, E.J.A., and Schedl, T. (2019). Biology of the Caenorhabditis elegans Germline Stem Cell System. Genetics *213*, 1145-1188.

Irnov, I., Wang, Z., Jannetty, N.D., Bustamante, J.A., Rhee, K.Y., and Jacobs-Wagner, C. (2017). Crosstalk between the tricarboxylic acid cycle and peptidoglycan synthesis in Caulobacter crescentus through the homeostatic control of alpha-ketoglutarate. PLoS Genet *13*, e1006978.

Jenkins, T.P., Rathnayaka, Y., Perera, P.K., Peachey, L.E., Nolan, M.J., Krause, L., Rajakaruna, R.S., and Cantacessi, C. (2017). Infections by human gastrointestinal helminths are associated with changes in faecal microbiota diversity and composition. PLoS One *12*, e0184719.
Kaval, K.G., and Garsin, D.A. (2018). Ethanolamine Utilization in Bacteria. mBio *9*.
Kocsisova, Z., Kornfeld, K., and Schedl, T. (2019). Rapid population-wide declines in stem cell number and activity during reproductive aging in C. elegans. Development *146*.

Kolde, R. (2015). pheatmap: Pretty Heatmaps. R package version 1.0. 8.
Korta, D.Z., Tuck, S., and Hubbard, E.J. (2012). S6K links cell fate, cell cycle and nutrient response in C. elegans germline stem/progenitor cells. Development *139*, 859-870.

Koyama, K. (2016). Bacteria-induced hatching of Trichuris muris eggs occurs without direct contact between eggs and bacteria. Parasitol Res *115*, 437-440.

Lee, S.C., Tang, M.S., Lim, Y.A., Choy, S.H., Kurtz, Z.D., Cox, L.M., Gundra, U.M., Cho, I., Bonneau, R., Blaser, M.J.*, et al.* (2014). Helminth colonization is associated with increased diversity of the gut microbiota. PLoS Negl Trop Dis *8*, e2880.

Liao, Y., Smyth, G.K., and Shi, W. (2014). featureCounts: an efficient general purpose program for assigning sequence reads to genomic features. Bioinformatics *30*, 923-930.

Love, M.I., Huber, W., and Anders, S. (2014). Moderated estimation of fold change and dispersion for RNA-seq data with DESeq2. Genome Biol *15*, 550.

Martin, P.K., Marchiando, A., Xu, R., Rudensky, E., Yeung, F., Schuster, S.L., Kernbauer, E., and Cadwell, K. (2018). Autophagy proteins suppress protective type I interferon signalling in response to the murine gut microbiota. Nat Microbiol *3*, 1131-1141.

Maruyama, R., Velarde, N.V., Klancer, R., Gordon, S., Kadandale, P., Parry, J.M., Hang, J.S., Rubin, J., Stewart-Michaelis, A., and Schweinsberg, P. (2007). EGG-3 regulates cell-surface and cortex rearrangements during egg activation in Caenorhabditis elegans. Current Biology *17*, 1555-1560.

Michaelson, D., Korta, D.Z., Capua, Y., and Hubbard, E.J. (2010). Insulin signaling promotes germline proliferation in C. elegans. Development *137*, 671-680.

Mok, D.Z., Sternberg, P.W., and Inoue, T. (2015). Morphologically defined sub-stages of C. elegans vulval development in the fourth larval stage. BMC Dev Biol *15*, 26.

Pacold, M.E., Brimacombe, K.R., Chan, S.H., Rohde, J.M., Lewis, C.A., Swier, L.J., Possemato, R., Chen, W.W., Sullivan, L.B., Fiske, B.P.*, et al.* (2016). A PHGDH inhibitor reveals coordination of serine synthesis and one-carbon unit fate. Nat Chem Biol *12*, 452-458.
Panesar, T. (1989). The moulting pattern in Trichuris muris (Nematoda: Trichuroidea). Canadian journal of zoology *67*, 2340-2343.

Parry, J.M., Velarde, N.V., Lefkovith, A.J., Zegarek, M.H., Hang, J.S., Ohm, J., Klancer, R., Maruyama, R., Druzhinina, M.K., and Grant, B.D. (2009). EGG-4 and EGG-5 link events of the oocyte-to-embryo transition with meiotic progression in C. elegans. Current Biology *19*, 1752-1757.
Pekar, O., Ow, M.C., Hui, K.Y., Noyes, M.B., Hall, S.E., and Hubbard, E.J.A. (2017). Linking the environment, DAF-7/TGFbeta signaling and LAG-2/DSL ligand expression in the germline stem cell niche. Development *144*, 2896-2906.

Penrod, J.T., and Roth, J.R. (2006). Conserving a volatile metabolite: a role for carboxysome-like organelles in Salmonella enterica. J Bacteriol *188*, 2865-2874.
Pepper, A.S., Lo, T.W., Killian, D.J., Hall, D.H., and Hubbard, E.J. (2003). The establishment of Caenorhabditis elegans germline pattern is controlled by overlapping proximal and distal somatic gonad signals. Dev Biol *259*, 336-350.

Ramanan, D., Bowcutt, R., Lee, S.C., Tang, M.S., Kurtz, Z.D., Ding, Y., Honda, K., Gause, W.C., Blaser, M.J., Bonneau, R.A.*, et al.* (2016). Helminth infection promotes colonization resistance via type 2 immunity. Science *352*, 608-612.

Rausch, S., Midha, A., Kuhring, M., Affinass, N., Radonic, A., Kuhl, A.A., Bleich, A., Renard, B.Y., and Hartmann, S. (2018). Parasitic Nematodes Exert Antimicrobial Activity and Benefit From Microbiota-Driven Support for Host Immune Regulation. Front Immunol *9*, 2282.

Roof, D.M., and Roth, J.R. (1989). Functions required for vitamin B12-dependent ethanolamine utilization in Salmonella typhimurium. J Bacteriol *171*, 3316-3323.

Rosa, B.A., Snowden, C., Martin, J., Fischer, K., Kupritz, J., Beshah, E., Supali, T., Gankpala, L., Fischer, P.U., Urban, J.F., Jr.*, et al.* (2021). Whipworm-Associated Intestinal Microbiome Members Consistent Across Both Human and Mouse Hosts. Front Cell Infect Microbiol *11*, 637570.

Rowley, C.A., Sauder, A.B., and Kendall, M.M. (2020). The ethanolamine-sensing transcription factor EutR promotes virulence and transmission during Citrobacter rodentium intestinal infection. Infection and immunity *88*, e00137-00120.

Roy, D., Kahler, D.J., Yun, C., and Hubbard, E.J.A. (2018). Functional Interactions Between rsks-1/S6K, glp-1/Notch, and Regulators of Caenorhabditis elegans Fertility and Germline Stem Cell Maintenance. G3 (Bethesda) *8*, 3293-3309.

Salinas, G., and Risi, G. (2018). Caenorhabditis elegans: nature and nurture gift to nematode parasitologists. Parasitology *145*, 979-987.

Schachter, J., Alvarinho de Oliveira, D., da Silva, C.M., de Barros Alencar, A.C.M., Duarte, M., da Silva, M.M.P., Ignacio, A., and Lopes-Torres, E.J. (2020). Whipworm Infection Promotes Bacterial Invasion, Intestinal Microbiota Imbalance, and Cellular Immunomodulation. Infect Immun *88*.

Sepulveda-Crespo, D., Reguera, R.M., Rojo-Vazquez, F., Balana-Fouce, R., and Martinez-Valladares, M. (2020). Drug discovery technologies: Caenorhabditis elegans as a model for anthelmintic therapeutics. Med Res Rev *40*, 1715-1753.

Shaham, S. (2006). WormBook. Methods in cell biology.

Simon-Manso, Y., Lowenthal, M.S., Kilpatrick, L.E., Sampson, M.L., Telu, K.H., Rudnick, P.A., Mallard, W.G., Bearden, D.W., Schock, T.B., Tchekhovskoi, D.V.*, et al.* (2013). Metabolite profiling of a NIST Standard Reference Material for human plasma (SRM 1950): GC-MS, LC-MS, NMR, and clinical laboratory analyses, libraries, and web-based resources. Anal Chem *85*, 11725-11731.

Smith, C.A., O'Maille, G., Want, E.J., Qin, C., Trauger, S.A., Brandon, T.R., Custodio, D.E., Abagyan, R., and Siuzdak, G. (2005). METLIN: a metabolite mass spectral database. Ther Drug Monit *27*, 747-751.

Sorrell, M.F., and Tuma, D.J. (1987). The functional implications of acetaldehyde binding to cell constituents. Ann N Y Acad Sci *492*, 50-62.

Spanier, B., Wallwitz, J., Zapoglou, D., Idrissou, B.M.G., Fischer, C., Troll, M., Petzold, K., and Daniel, H. (2018). The Reproduction Rate of Peptide Transporter PEPT-1 Deficient C. elegans Is Dependent on Dietary Glutamate Supply. Front Mol Biosci *5*, 109.

Starich, T.A., Bai, X., and Greenstein, D. (2020). Gap junctions deliver malonyl-CoA from soma to germline to support embryogenesis in Caenorhabditis elegans. Elife *9*.

Thomason, L.C., Costantino, N., and Court, D.L. (2007). E. coli Genome Manipulation by P1 Transduction. Current Protocols in Molecular Biology *79*, 1.17.11-11.17.18.

Virtanen, P., Gommers, R., Oliphant, T.E., Haberland, M., Reddy, T., Cournapeau, D., Burovski, E., Peterson, P., Weckesser, W., Bright, J.*, et al.* (2020). SciPy 1.0: fundamental algorithms for scientific computing in Python. Nat Methods *17*, 261-272.

Vos, T., Allen, C., Arora, M., Barber, R.M., Bhutta, Z.A., Brown, A., Carter, A., Casey, D.C., Charlson, F.J., and Chen, A.Z. (2016). Global, regional, and national incidence, prevalence, and years lived with disability for 310 diseases and injuries, 1990–2015: a systematic analysis for the Global Burden of Disease Study 2015. The lancet *388*, 1545-1602.

White, E.C., Houlden, A., Bancroft, A.J., Hayes, K.S., Goldrick, M., Grencis, R.K., and Roberts, I.S. (2018). Manipulation of host and parasite microbiotas: Survival strategies during chronic nematode infection. Sci Adv *4*, eaap7399.

Yeates, T.O., Crowley, C.S., and Tanaka, S. (2010). Bacterial microcompartment organelles: protein shell structure and evolution. Annu Rev Biophys *39*, 185-205.

Yuen, L.H., Saxena, N.S., Park, H.S., Weinberg, K., and Kool, E.T. (2016). Dark Hydrazone Fluorescence Labeling Agents Enable Imaging of Cellular Aldehydic Load. ACS Chem Biol *11*, 2312-2319.